Enhancement of Transmission Line Theory for Finite-Length Non-Uniform Transmission Lines Using Scattering Theory

by

Manuja Shamith Gunawardana Sooriyaarachchige Don

A thesis submitted to the Faculty of Graduate Studies of
The University of Manitoba
in partial fulfilment of the requirements of the degree of

Master of Science

Department of Electrical and Computer Engineering
University of Manitoba
Winnipeg, Canada

Examining Committee

This thesis was examined and approved by the following examining committee on December 18, 2018:

- **Prof. B. Kordi** (advisor)

  Department of Electrical & Computer Engineering

  University of Manitoba

- **Prof. V. Okhmatovski**

  Department of Electrical & Computer Engineering

  University of Manitoba

- **Prof. M. Birouk**

  Department of Mechanical Engineering

  University of Manitoba

Abstract

Classical multiconductor transmission line (MTL) theory is valid for infinitely-long, uniform transmission lines whose cross sectional dimensions are very small compared to the minimum wavelength. Therefore, non-uniformities such as bends, crossings, conductors of different lengths, or electrically distant conductors are not represented in classical MTL models.

The proposed scattering based coupling (SBC) method, which uses electromagnetic scattering theory to model mutual coupling between conductors, has been used to model differently-lengthed and electrically distant parallel conductors. Scattered field transmission line (SFTL) model which regards both self and mutual fields to be scattered fields, has been used to model lossless, frequency-independent conductors, that crosses each other at variable crossing angles and for bent conductors at variable bending angles. The SBC and SFTL models have been compared with full-wave thin wire and full-wave, 3D-FEM solvers, respectively.

Acknowledgements

Firstly, I would like to express my gratitude to my advisor Dr. Behzad Kordi for his guidance motivation and encouragement throughout my M.Sc. He always makes sure that his students work in a stress free environment an it's always a pleasure to work with him.

Many thanks to my thesis committee, Dr. Vladimir Okhmatovski and Dr. Madjid Birouk for their comments and suggestions to improve my thesis.

Financial support from University of Manitoba, Faculty of Graduate Studies and Natural Sciences and Engineering Research Council of Canada (NSERC) is gratefully acknowledged. I would also like to express my gratitude to the Government of Manitoba for the financial support received in the form of Graduate Scholarship.

Last but not least, I would like to thank my family and friends. Many sincere thanks to my parents and my sister for their kindness and support while I was pursuing my studies away from them. Many thanks to my friends in Winnipeg, who have been immensely supportive through my ups and downs.

Dedication

To my loving parents and sister.

Table of Contents

List of Figures

Chapter 1

Introduction

1.1 Motivation

Transmission lines play a vital role in a power system by transmitting electrical energy over large distances. In addition to the power frequency voltage, transient over-voltages produced by various causes including switching operations, lightning strikes, and short circuit faults, also get transmitted through transmission lines [1]. These transients can cause damage to power system components which are connected via transmission lines and result in massive repair and/or replacement costs. Transients travelling in power lines can also induce electromagnetic interference on other power lines and communication lines in close proximity [2, 3]. Therefore, it is essential to accurately model a transmission network in order to understand the transient behaviour of a power system at the design stage as well as, during operation and fault identification.

The widely used method to include transmission lines in power system, electromagnetic transient (EMT) type simulation models is to use multi-conductor transmission line (MTL)

theory based on the Telegrapher's equations and transverse electromagnetic (TEM) mode of propagation [4]. Apart from power transmission lines, MTL models are also used to analyse a wide variety of structures ranging from transformer windings to interconnects of an electronics chip [5–7]. However, since the TEM mode is only valid for a system of infinitely long, uniform conductors [4], classical MTL theory cannot be used to model non-uniformities in wire structures [8].

As transmission networks keep expanding, lines in them tend to interact more with other power lines and communication networks in close proximity, influencing the transient behaviour of each other. Therefore, more detailed modelling has become a necessity in order to understand the transient behaviour of a transmission line network.

1.2 Problem Definition and Conventional Solutions

Non-uniformities that can cause interference on the transmission network such as bends in transmission lines or crossings between two power lines or a power line and a communication line, as shown in Fig. 1.1, appear frequently in power systems. Full-wave electromagnetic analysis done on bus-bars in gas insulated switchgear (GIS) in [9] shows a reflected current of approximately 0.1 times of the original excitation occurring at a 90° bend. As transmission networks keep expanding, more such non-uniformities get added to the network. However, current EMT simulation models for transmission lines are unable to represent these situations. Apart from such situations pertinent to power transmission lines, cases where the coupled wires are not of equal length, and/or where they are placed electrically distant from each other (but close to ground) frequently happen in transformer windings and microstrip circuits which again cannot be represented using classical MTL models. Therefore, to an-

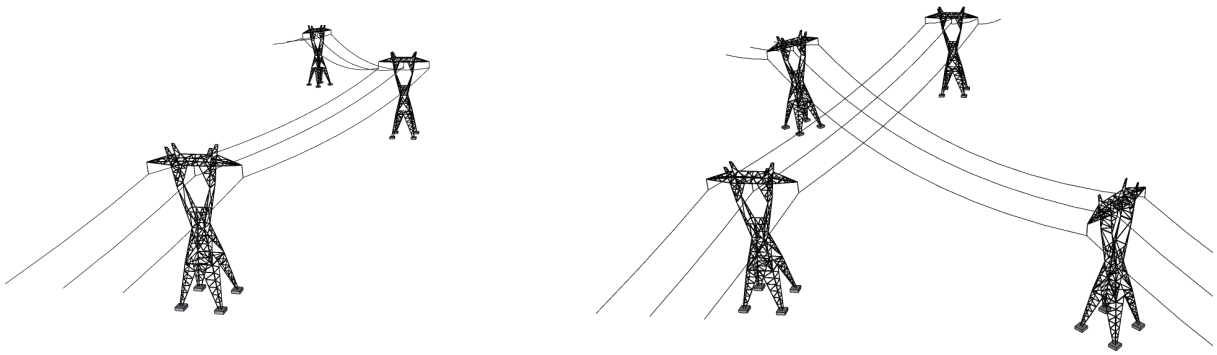

Fig. 1.1: A schematic of a (a) power line bend and (b) crossing.

alyze the crosstalk between wires of such cases an enhancement to the classical model is required.

Although, the most accurate method to model these situations is to use full-wave techniques [10–12], they are computationally cumbersome, which makes them hardly compatible with power system simulation tools. Most of these techniques are in frequency-domain and time-domain implementation is usually performed using numerical techniques such as three dimensional finite element method (FEM) and finite-difference time-domain (FDTD). Most of the research done in the field of electro-magnetics in this regard, have been on high frequency applications and therefore do not possess closed form equations to represent non-uniform structures [13,14]. Here, high frequencies are where the transverse dimensions of the line are comparable with the minimum significant wavelength of the exciting electromagnetic field [15]. Not having closed form solutions, introduces the requirement of iterative methods to arrive at a solution which is undesirable for power system transient simulators.

1.3 Objective of the Thesis

The objective of this thesis is to develop methods to include these non-uniformities into transmission line models while preserving their computational simplicity. As mentioned in the previous section, since the Telegrapher's equations are unable to incorporate any non-uniform cross-section, electromagnetic scattering theory has to be used to determine the governing equations of the exciting electromagnetic field. Scattering theory allows to incorporate the change in electromagnetic fields close to a non-uniformity.

Electromagnetic scattering equations, in their raw form, have integral terms which do not have an analytical solution and therefore are computationally complex. This research focusses on simplifying the initial formulae developed using scattering theory into closed-forms, by taking into account the typical geometrical and frequency characteristics of transmission lines. The developed models are to be implemented into a finite-difference-time-domain (FDTD) [4, 8] algorithm, so that they can be integrated in EMT simulators.

1.4 Research Contributions

The contributions of this thesis are as follows:

- Development of a scattering based coupling (SBC) model which is a closed-form frequency-domain model to solve parallel conductors of different lengths and electrically distant conductors. Time-domain results have been obtained using the inverse Fourier Transform.
- Comparison of SBC model with a commercial thin-wire, full-wave solver (Numerical Electromagnetic Code - NEC) [16].

- Development of a scattered field transmission line (SFTL) model which is a closed-form time-domain model for transmission line crossings and bends for lossless, frequency independent conductors.
- Implementation of the developed model using a 1D-FDTD algorithm, which is suitable to be integrated into EMT simulators.
- Comparison of SFTL model with a 3D, full-wave, finite-element (FEM) solver

1.4.1 Publications

Work conducted on the SBC model was submitted to and presented as a conference paper at Progress In Electromagnetic Research Symposium (PIERS) - 2018. The main focus of the paper was on the development of a closed-form model for parallel conductors of different lengths, placed electrically close or far from each other, and comparison of results with full-wave theory. This paper received the Best Student Paper Award in the subcategory for Computational Electromagnetics, Electromagnetic Compatibility, Scattering and Electromagnetic Theory and the Young Scientist Award at the conference.

A journal paper based on the SFTL model has been prepared to be submitted to IEEE transactions on power delivery. This paper includes the development of the SFTL model for transmission line crossings, implementation of the developed model using a FDTD algorithm and comparison of the obtained results with those obtained using full-wave theory.

1.5 Thesis Outline

This thesis is divided in to 4 chapters as defined below:

Chapter 1: Introduction, background information, problem definition and existing solutions, objectives, and contributions.

Chapter 2: Literature review of this study completed on classical MTL models, their limitations, non-uniform line models based on MTL theory and scattering theory.

Chapter 3: Development of the scattering based coupling MTL model for electrically distant conductors with different lengths, and comparison of it's results with full-wave theory.

Chapter 4: Development of the scattered field transmission line model for finite-length, transmission line crossings and bends. Discussion on the FDTD algorithm for solving the developed equations is presented and the results obtained from the developed model are compared with full-wave theory.

Chapter 5: Conclusion of this thesis project, with a discussion on future work.

Chapter 2
Literature Review

2.1 Classical MTL Models

For a wire structure as shown in Fig. 2.1, classical multi-conductor transmission line (MTL) equations are obtained assuming a transverse electro-magnetic (TEM) field structure. In the TEM mode, the electric and magnetic fields are assumed to exist only on the transverse plane which is perpendicular to the axis of the wire and wave propagation is assumed to occur only along the wire axis. The MTL equations in the frequency-domain are given by [4]

$$\frac{\mathrm{d}}{\mathrm{d}z}\begin{bmatrix}\boldsymbol{V}(z,j\omega)\\ \boldsymbol{I}(z,j\omega)\end{bmatrix} = -\begin{bmatrix}\boldsymbol{Z} & 0\\ 0 & \boldsymbol{Y}\end{bmatrix}\begin{bmatrix}\boldsymbol{V}(z,j\omega)\\ \boldsymbol{I}(z,j\omega)\end{bmatrix} \tag{2.1}$$

where

$$\boldsymbol{Z} = \boldsymbol{R} + j\omega\boldsymbol{L}$$

$$\boldsymbol{Y} = \boldsymbol{G} + j\omega\boldsymbol{C}.$$

$\boldsymbol{V}(z,j\omega)$ and $\boldsymbol{I}(z,j\omega)$ are the voltage and current vectors at any location z. The matrices $\boldsymbol{R},\boldsymbol{L},\boldsymbol{G}$ and $\boldsymbol{C}$ are the per unit length (PUL) resistance, inductance, conductance and

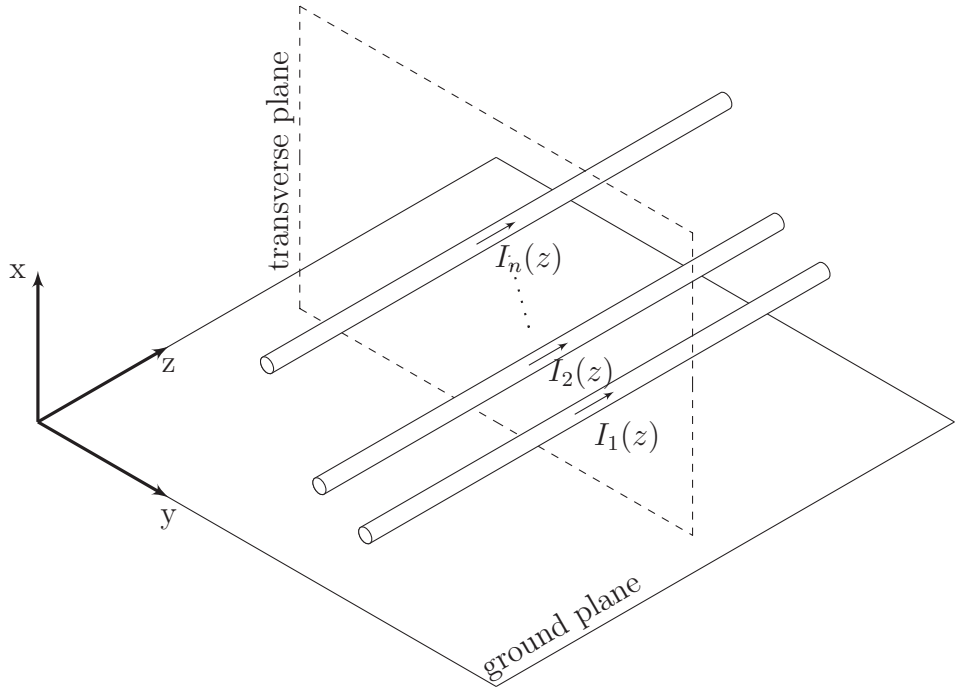

Fig. 2.1: TEM mode in a multi-conductor system.

capacitance matrices, respectively. The PUL impedance ($\boldsymbol{Z}$), and admittance ($\boldsymbol{Y}$) matrices in these equations are assumed to be fixed along the length of the line and are calculated for the cross-section of a uniform, infinitely-long transmission line.

The simplicity of MTL models, compared to full-wave analysis, where waves propagate in a three dimensional space, and the availability of an analytical solution allowed these models to be used for frequency-domain analysis of transmission lines, as early as, in 1950's [17]. The solution for (2.1) can be obtained using its analogy to state-variable formulation and are given by [4]

$$\begin{bmatrix} \boldsymbol{V}(z) \\ \boldsymbol{I}(z) \end{bmatrix}_{2n\times 1} = \Big[\boldsymbol{\Phi}(z-z_0)\Big]_{2n\times 2n} \begin{bmatrix} \boldsymbol{V}(z_0) \\ \boldsymbol{I}(z_0) \end{bmatrix}_{2n\times 1} \tag{2.2}$$

where,

$$[\boldsymbol{\Phi}(z)]_{2n\times 2n} = e^{\boldsymbol{A}z}$$

and

$$\boldsymbol{A} = \begin{bmatrix} \boldsymbol{0} & -\boldsymbol{Z} \\ -\boldsymbol{Y} & \boldsymbol{0} \end{bmatrix}.$$

In (2.2), z and z_0 are the two ends of the length of a segment of the line. $\boldsymbol{\Phi}$ is commonly known as the chain-parameter matrix in transmission line theory [4].

In the 1970's, considerations of the electromagnetic compatibility (EMC) community, of how the communication networks would react to an external electromagnetic pulse [17], lead to an important development in the MTL theory. Incident field excitations were added to the classical MTL equations in (2.1) as [18–20],

$$\frac{\mathrm{d}}{\mathrm{d}z}\begin{bmatrix} \boldsymbol{V}(z,j\omega) \\ \boldsymbol{I}(z,j\omega) \end{bmatrix} = -\begin{bmatrix} \boldsymbol{Z} & 0 \\ 0 & \boldsymbol{Y} \end{bmatrix}\begin{bmatrix} \boldsymbol{V}(z,j\omega) \\ \boldsymbol{I}(z,j\omega) \end{bmatrix} + \begin{bmatrix} \boldsymbol{V}_F(z,j\omega) \\ \boldsymbol{I}_F(z,j\omega) \end{bmatrix} \tag{2.3}$$

where $\boldsymbol{V}_F(z,j\omega)$ and $\boldsymbol{I}_F(z,j\omega)$ are the distributed incident voltage and current. Solution for these equations are given by.

$$\begin{bmatrix} \boldsymbol{V}(z) \\ \boldsymbol{I}(z) \end{bmatrix} = \Big[\boldsymbol{\Phi}(z-z_0)\Big]\begin{bmatrix} \boldsymbol{V}(z_0) \\ \boldsymbol{I}(z_0) \end{bmatrix} + \int_{z_0}^{z}\Big[\boldsymbol{\Phi}(z-z')\Big]\begin{bmatrix} V_F(z') \\ I_F(z') \end{bmatrix} dz'. \tag{2.4}$$

In the late 1970's, with the development of digital electronics, an interest for time-domain analysis aroused [17], which involved the solution of,

$$\frac{\mathrm{d}}{\mathrm{d}z}\begin{bmatrix} \boldsymbol{V}(z,t) \\ \boldsymbol{I}(z,t) \end{bmatrix} = -\frac{\mathrm{d}}{\mathrm{d}t}\begin{bmatrix} \boldsymbol{L} & 0 \\ 0 & \boldsymbol{C} \end{bmatrix}\begin{bmatrix} \boldsymbol{V}(z,t) \\ \boldsymbol{I}(z,t) \end{bmatrix} \tag{2.5}$$

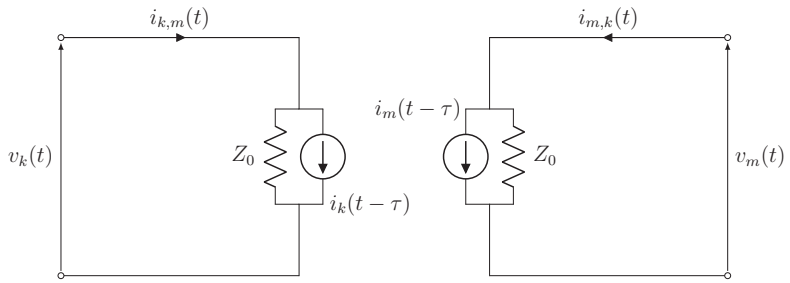

Fig. 2.2: SPICE equivalent circuit for a single-conductor, loss-less transmission line.

For loss-less lines as described in (2.5), an analytical solution is achievable, while in the case of lossy transmission lines there is no such solution [4]. With the development of SPICE software, an equivalent circuit model with distributed L and C, has been developed and implemented for lossless lines as explained in [4]. Fig. 2.2 depicts the SPICE circuit model for a single conductor loss-less line. m and k refer to the two ends, and Z_0 to the characteristic impedance of the line. Here, single conductor refers to one conductor with ground as the return path. In this circuit model the terminal voltage and current at one end of the line at a particular time (t) can be computed using the terminal voltage and current of the other end of the line.

This mechanism paved the way for circuit simulators to analyse transients in transmission lines in the time-domain. Incorporation of losses is approximated by adding lumped resistances at the two ends as well as the middle of a lossless transmission line as shown in Fig. 2.3 which can be reduced to the original form as Fig. 2.4. This model is well known as Bergeron's model [21] and is commonly used in EMT type simulators [22, 23].

Classical MTL theory has its own limitations owing to the assumptions on which it is based on. The assumption that every cross-section, including the terminals, have the same Z and Y characteristics, limits the application of classical MTL theory only to parallel

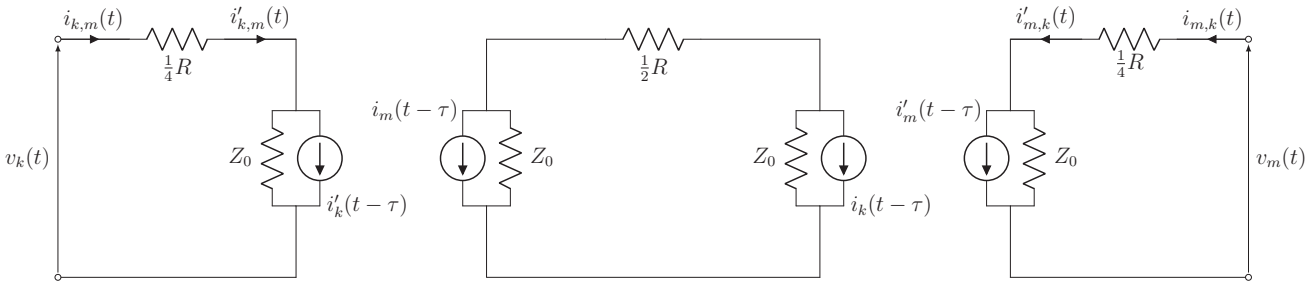

Fig. 2.3: Inclusion of losses to the SPICE equivalent circuit.

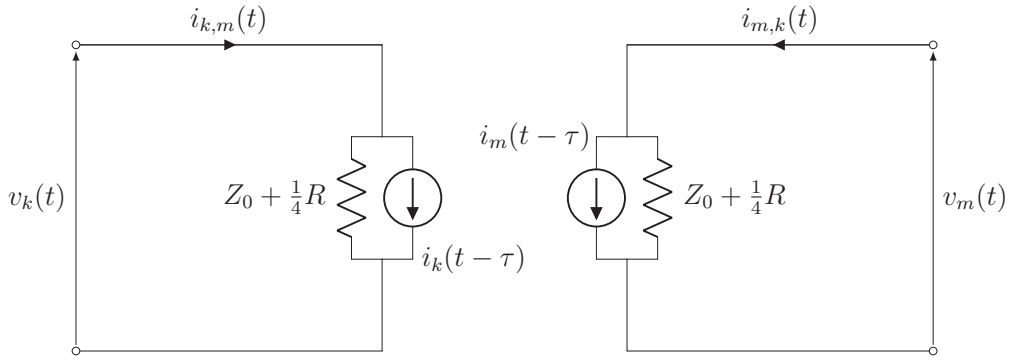

Fig. 2.4: Bergeron's model for a lossy single-conductor transmission line.

conductors spanning the same length. The TEM mode of propagation, assumes the coupling between conductors is instantaneous and therefore, all conductors should be electrically close (maximum cross-sectional dimension should not exceed 0.1 of the highest frequency wavelength) in order for the MTL theory to be valid. Therefore, classical MTL models are unable to simulate a non-uniformity occurring at a particular location on a transmission line. In other words, current power system EMT models assume the transmission lines to be straight conductors with no excitation from external sources.

2.2 Non-uniform line models based on transmission line theory

As mentioned in the previous section, the MTL equations assume a uniform structure and non-varying PUL parameters with space. However, in a case where the cross sectional format changes along the line, such as in bends, crossings and other non-uniformities, the PUL parameters become functions of the position variable and cause the MTL equations to take the format of [4]

$$\frac{\mathrm{d}}{\mathrm{d}z}\begin{bmatrix}\boldsymbol{V}(z,j\omega)\\ \boldsymbol{I}(z,j\omega)\end{bmatrix} = -\begin{bmatrix}\boldsymbol{Z}(z) & 0\\ 0 & \boldsymbol{Y}(z)\end{bmatrix}\begin{bmatrix}\boldsymbol{V}(z,j\omega)\\ \boldsymbol{I}(z,j\omega)\end{bmatrix}. \tag{2.6}$$

These resulting non-uniform transmission line (NTL) equations are very difficult to solve due to the non-constant coefficients. The common way to handle such a situation is to divide the non-uniform line into a cascade of uniform sections [4]. However, this approach is applicable only for some geometries and in some cases it can cause unwanted reflections if the transition between sections is not smooth enough.

Ametani *et al.* have used the approach above to model non-parallel transmission lines above ground [24]. In this work, two non-parallel conductors have been modelled as a cascade of multiple parallel sections as shown in Fig. 2.5. The impedance and admittance of each section have been calculated using Carson-Pollaczek's impedance and space admittance [25, 26] formulae which assume the conductors are infinitely long. Cases where the interconnections between sections are represented as short circuits, (Fig. 2.5a), and as vertical transmission line segments (Fig. 2.5b) have been analyzed. The interconnections have been assumed to have zero coupling with the other conductor (conductor a in Fig. 2.5b). As discussed in the paper, segmenting the inclined wire changes its length and affects its travel time if not addressed properly. The perpendicular connections between sections have also found to be adding unwanted oscillations due to reflections, since they appear as distinct discontinuities along the line. Cascaded uniform-lines have been successfully used in [27] for modelling exponentially and linearly tapered lossy transmission lines.

In [28,29] Ametani *et al.* have developed a closed-form, space dependent PUL impedance for a finite-length inclined line above ground, based on the method of images [30]. The study shows that the PUL impedance gradually drops as we get closer to end of the transmission line due to the lowering of conductors to connect to the substation bus. In [31], the closed-form formula developed in [28] has been used to model two non-parallel conductors in free space, and a single inclined conductor above ground using a 3D-FDTD solver.

A non-uniform, lossless, exponential transmission line has been modelled in the time-domain in [32]. An equivalent circuit has been developed with the intention of including the developed model in an EMT-type simulator. An exponential transmission line is explained as a transmission line having governing equations in the frequency-domain as,

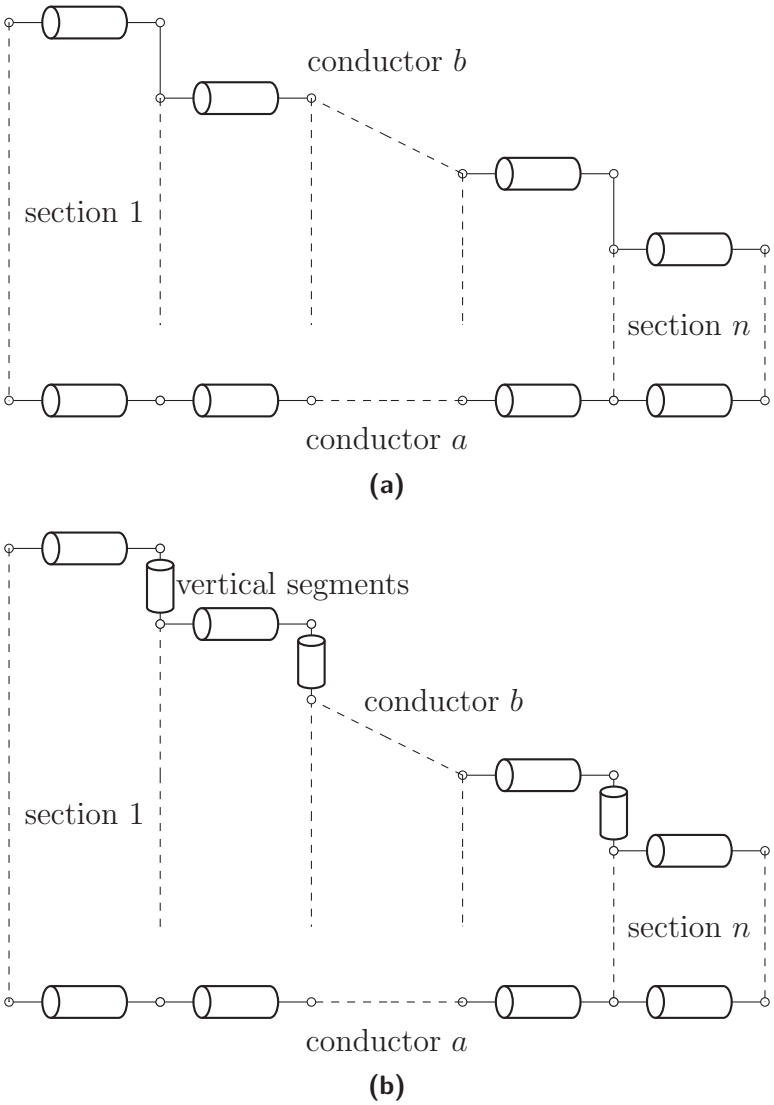

Fig. 2.5: Ametani's representation of non-parallel transmission lines (a) with and (b) without vertical segments [24].

$$\frac{\mathrm{d}V(z)}{\mathrm{d}z} = -j\omega L_0 e^{qz} I(z) \tag{2.7a}$$

and

$$\frac{\mathrm{d}I(z)}{\mathrm{d}z} = -j\omega C_0 e^{-qz} V(z) \tag{2.7b}$$

where L_0 and C_0 are PUL inductance and capacitance at $z = 0$ and q is the decaying factor. However, an exponential line is a special case of non-uniform transmission lines which not only has analytical PUL parameters but also has an analytical solution in the frequency-domain. Other such cases where an analytical solution is attainable are binomial, power law and Hermite transmission lines [33–35]. However, there are numerous other cases where closed-form PUL parameters and/or analytical solutions might not be available due to the complexity of the electromagnetic fields generated and the geometry of the transmission line.

A frequency-domain model for non-uniform transmission lines with known PUL parameters which can be represented by converging Taylor series has been developed in [36]. An analytic solution in frequency-domain for tapered transmission lines with triangular and exponential characteristic impedances has been obtained in [37]. In [38], an iterative and adaptive perturbation technique for the analysis of non-uniform transmission lines has been presented where the space dependent variations of the p.u.l parameters have been interpreted as perturbations with respect to their average values. In all of the above researches, the existence of a closed-form function to represent PUL parameters has been critical for arriving at a solution analytically or numerically.

Finite-Difference Time-Domain (FDTD) methods [39] have been widely used to solve many electromagnetic problems including full-wave models [29,40]. Single-dimensional FDTD as explained in [4], where the MTL equations are discretized in both time and space, is a

common way of handling lossy and non-uniform transmission lines. Lossy lines have been modelled using FDTD in [41–43]. Watanabe *et al.* has developed an FDTD model for a single conductor transmission line with known space-varying cross-sectional dimensions in [44]. An efficient FDTD algorithm which does not require the Courant-Friedrich-Levy (CFL) stability condition [4] has been presented for lossy, non-uniform lines in [45].

Unlike Bergeron's method, the FDTD method doesn't need to decouple MTLs before solving, which makes the formulation simple and easier to implement. Inclusion of non-uniformities as space varying PUL parameters is straight-forward since the total length is descretized into small segments. Differential terms in the MTL equations are handles using finite difference methods. Frequency dependent cases can also be analysed by recursive convolutions as explained in [46]. In [46], Kordi *et al.* has also integrated the developed FDTD model for a frequency dependent transmission line into a power system EMT-simulator. This suggests that FDTD is a viable candidate for implementing non-uniform transmission lines in EMT-type simulators, provided that the non-uniformities could be represented in closed-forms, or at least as recursive convolutions.

2.3 Non-uniform Line Models Using Scattering Theory

As explained in the previous section, not much effort has been made on including non-uniform transmission lines into power system EMT-type simulators. However, non-uniformities on transmission lines, such as bends, junctions, or crossing have continuously been a subject of interest in the electromagnetic compatibility (EMC) community since they occur frequently in electromagnetic devices. Most models found in the literature in this regard are built on electromagnetic scattering equations in the frequency-domain.

A source connected directly or an incident field can cause currents and charges to flow in a conductor. These currents and charges can in turn create another electric and magnetic field which are referred to as scattered fields. The scattered electric field produced by a thin-wire of length ℓ can be expressed in terms of vector and scalar potentials as [15],

$$\boldsymbol{E}^s = -j\omega\boldsymbol{A} - \nabla\Phi \tag{2.8}$$

with

$$\boldsymbol{A}(\boldsymbol{r}) = \frac{\mu}{4\pi}\int_0^\ell I(z')\hat{a}_z g\left(\boldsymbol{r},\boldsymbol{r}'\right)dz'$$

and,

$$\Phi(\boldsymbol{r}) = \frac{1}{4\pi\varepsilon}\int_0^\ell \rho(z')g\left(\boldsymbol{r},\boldsymbol{r}'\right)dz'$$

where z' is the length variable along the axis of wire, $\boldsymbol{r} = x\hat{a}_x + y\hat{a}_y + z\hat{a}_z$ is the position vector of the observation point and $\boldsymbol{r}'$ is the position vector of the source. $I(z')$ and $\rho(z')$ are the current and charge density along the wire. $g\left(\boldsymbol{r},\boldsymbol{r}'\right)$ is the scalar Green's function which will be explained in the next sections. It is a common practice in scattering problems to select $\boldsymbol{r}'$ to be on the wire axis and $\boldsymbol{r}$ to be on the wire surface or further as shown in Fig. 2.6 to avoid singularity in the Green's function [47]. Scattering equations are not uniform in space as Telegrapher's equations, which makes them applicable for more general cases. However, they generally do not possess an analytical solution and therefore are computationally cumbersome.

Kami *et al.* has proposed a frequency-domain coupling model for crossing, thin-wire, two-conductor transmission lines over perfect electrical conducting (PEC) ground in [48]. Each conductor has been modelled using the Taylor's coupling model [18]. The mutual

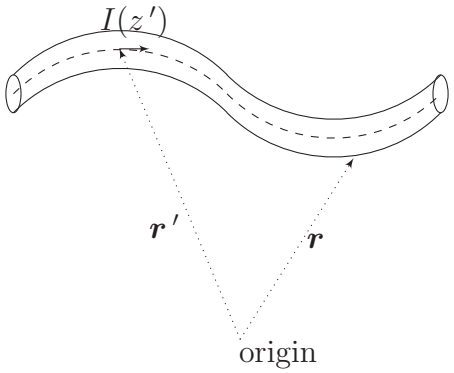

Fig. 2.6: Placement of source point and observation point in a scattering problem.

coupling between conductors has been included using the incident fields as,

$$-\frac{\mathrm{d}}{\mathrm{d}z_i}\begin{bmatrix} V(z_i,j\omega) \\ I(z_i,j\omega) \end{bmatrix} = \begin{bmatrix} j\omega L_i & 0 \\ 0 & j\omega C_i \end{bmatrix}\begin{bmatrix} V(z_i,j\omega) \\ I(z_i,j\omega) \end{bmatrix} + \begin{bmatrix} j\omega A^e_{z_i}(z_i, x=h_j) \\ -j\omega C_i \Phi^e(z_i, x=h_j) \end{bmatrix} \tag{2.9}$$

where i and j refer to the two conductors, and A^e and Φ^e to the external scalar and vector potential created by the nearby conductor in the absence of the considered conductor. Electromagnetic scattering theory under thin-wire approximation and low frequency has been used to derive the incident electric and magnetic fields. Equations have been solved based on the assumption that the re-coupling from the line under induction (acceptor line) is negligible compared to the self excitation on the exciter line. This would consider any reflections occurring on the exciter line at the point of crossing to be zero. However, according to the study done in this thesis project using full-wave solvers, it is evident that the exciter line can contain reflections of considerable amplitude depending on the distance of gab between conductors crossing each other.

Using the same approach as above, a frequency-domain model for an arbitrarily directed

system of thin-wires has been developed in [49] as

$$\begin{bmatrix} V_i(0) \\ \\ I_i(0) \end{bmatrix} = \begin{bmatrix} \cos\beta\ell_i & jZ_0\sin\beta\ell_i \\ \\ j\dfrac{1}{Z_0}\sin\beta\ell_i & \cos\beta\ell_i \end{bmatrix} \begin{bmatrix} V_i(\ell_i) \\ \\ I_i(\ell_i) \end{bmatrix} + \sum_{j=1,j\neq i}^{n} \int_0^{\ell_j} \begin{bmatrix} \cos\beta z' & jZ_0\sin\beta z' \\ \\ j\dfrac{1}{Z_0}\sin\beta z' & \cos\beta z' \end{bmatrix} \begin{bmatrix} V_{F_j}(z') \\ \\ I_{F_j}(z') \end{bmatrix} dz' \tag{2.10}$$

where,

$$\begin{bmatrix} V_{F_j}(z') \\ \\ I_{F_j}(z') \end{bmatrix} = \begin{bmatrix} -j\omega\displaystyle\int_0^h \left(\frac{\partial A_{x_j}}{\partial z} + \frac{\partial A_{z_j}}{\partial x}\right) dx' \\ \\ C_i\left(\omega^2\displaystyle\int_0^h A_{x_j}dx' + \frac{\Delta\cdot\boldsymbol{A}_j}{\mu\varepsilon}\Big|_{x'=0}^{x'=h}.\right) \end{bmatrix},$$

which has been used in [50] to model bent multi-conductor thin-wire systems. This formulation also includes the coupling from the risers that are connected to the terminals. Coupling terms of these models, which have been obtained using scattered fields are in the integral form that do not have a closed-form and therefore are not compatible with circuit simulators. Both these models consider the self excited propagation in each line to be of TEM mode, and only the coupling is modelled using scattering theory. For better accuracy, other researchers have developed full-scattering models to handle these non-uniformities.

Tkatchenko *et al.* have developed transmission-line-like equations for a finite-length line above PEC ground in [13] using the scattering theory. Under the assumption that the electric

and magnetic fields only lie on the transverse plane we can write,

$$\hat{a_z} \cdot \boldsymbol{E}^s = 0 \tag{2.11}$$

where $\hat{a_z}$ the unit vector in z direction, and $\boldsymbol{E}^s$ is the scattered electric field. Using the equations given in (2.8) and (2.11) the field-to-transmission-line equations for a finite length wire of length ℓ has been obtained as [13]

$$\frac{\mathrm{d}V(z)}{\mathrm{d}z} + j\omega\frac{\mu}{4\pi}\int_0^\ell g\,(z,z')\,I(z')dz' = \boldsymbol{E}_z^s(h,z) \tag{2.12a}$$

$$\frac{\mathrm{d}}{\mathrm{d}z}\int_0^\ell g\,(z,z')\,I(z')dz' + j\omega 4\pi\varepsilon V(z) = 0. \tag{2.12b}$$

In (2.12), $\boldsymbol{E}_z^s(h,z)$ is the incident electric field at the height of the wire h. It is explained that at low frequencies equations (2.12a) and (2.12b) can be simplified into well-known Telegrapher's equations for regions which are not close to the terminals. Here, low frequencies are where $k \cdot h \ll 1$. h is the height of the conductor from the ground and k is the wave number related that is to the angular frequency ω by $k = \omega/c$. However, the regions within $2h$ distance from the ends, deviate from the TEM mode. Since the purpose of the research in [13] has been on analyzing field coupling at high frequencies, the scattering equations have not been simplified from their original form. The integral terms in (2.12) that includes the scalar Green's functions does give a more accurate representation compared to the constant PUL parameters in Telegrapher's equations. However, they do not have a closed-form and therefore, an iterative method based on the perturbation theory has been used to arrive at solutions in the frequency-domain.

In [14], a similar model for a single-conductor line with a bend (of variable angle) has been

developed by the same researchers, that also uses an iterative method to arrive at a solution in the frequency-domain. Chunfei *et al.*, in [51], have developed a non-uniform transmission line approach for modelling bends starting from the scattering equations in the frequency-domain. The scattering equations are simplified to space-varying PUL parameters. However, as discussed in [51], the PUL parameters need to be calculated using numerical integration or exponential integration, which are both computationally inefficient than having an analytical solution.

2.4 Summary

Classical MTL models are being widely used for the transient analysis of transmission lines in EMT-type simulators owing to their simplicity and availability of analytic solutions. Classical models assume transmission lines to have a uniform cross-section along their entire span. On the other hand real transmission lines contain non-uniformities such as bends and crossings.

Modelling of non-uniform transmission lines is a challenging task since their governing equations do not have analytical solutions except for a few special cases. However, if the non-uniformities can be expressed in terms of closed-form functions, numerical techniques such as FDTD can be used to solve them in time-domain.

Non-uniform wire structures can be accurately formulated using scattering theory, but they contain integral terms that do not possess analytical solutions in their raw form. Most scattering models are aimed for high-frequency applications and therefore do not simplify their integrals, and instead use iterative methods to arrive at the solution in the frequency-domain.

Chapter 3

Scattering Based Coupling (SBC) Model

In this chapter the development of a frequency-domain model for parallel conductors of different lengths and electrically distant conductors is presented. The frequency-domain solution of the developed model is obtained analytically, while the time-domain solution is obtained using the inverse Fourier transform. In the proposed model, each conductor of an MTL is modelled as a single-conductor transmission line (STL) and the coupling from the other conductors is included into the STL equations as external electric and magnetic fields. The solution of all STL equations are combined into a system of matrix equations whose structure is similar to that of an MTL model with a chain parameter matrix as explained in [50]. Closed-form formulae for parallel conductors are obtained which has the same computational complexity of a classical MTL model. Incorporation of terminal constraints is done similar to MTL models. Scattering theory is employed to model the coupling from external fields. The proposed model is used to model three cases of two parallel, lossless conductors above PEC ground. Results obtained using the proposed model are presented along with those obtained using numerical electromagnetic code (NEC).

3.1 Representation of the Mutual Coupling as Incident Fields

Using Taylor coupling model, the transmission line equations for a conductor with incident field excitation are given by [18]

$$\frac{\mathrm{d}V_i(z)}{\mathrm{d}z} + j\omega L_i I_i(z) = -j\omega \int_0^h B_y^{\mathrm{inc}} dx' \tag{3.1a}$$

and

$$\frac{\mathrm{d}I_i(z)}{\mathrm{d}z} + j\omega C_i V_i(z) = -j\omega C_i \int_0^h E_x^{\mathrm{inc}} dx' \tag{3.1b}$$

where $V_i(z)$ and $I_i(z)$ are voltage and current at any position z, and L_i and C_i are per unit length inductance and capacitance of the i^{th} line. B_y^{inc} and E_x^{inc} are the incident magnetic and electric fields due to other conductors of the MTL. The magnetic and electric fields can be represented using magnetic vector potential using Lorentz gauge [30] using [8]

$$\mathbf{B} = \nabla \times \mathbf{A} \tag{3.2}$$

$$\mathbf{E} = \frac{1}{j\omega\mu\epsilon}\nabla^2\mathbf{A} - j\omega\mathbf{A}. \tag{3.3}$$

Using (3.2) and (3.3), (3.1) can be re-written and simplified as

$$\frac{\mathrm{d}V_i(z)}{\mathrm{d}z} + j\omega L_i I_i(z) = j\omega A_{z,z}^{\mathrm{inc}}\Big|_{x'=0}^{x'=h_i} \tag{3.4a}$$

and

$$\frac{\mathrm{d}I_i(z)}{\mathrm{d}z} + j\omega C_i V_i(z) = \frac{C_i}{\mu\epsilon}\left(\frac{\partial A_{z,z}^{\mathrm{inc}}}{\partial z} + \frac{\partial A_{y,z}^{\mathrm{inc}}}{\partial y}\right)\Big|_{x'=0}^{x'=h_i}. \tag{3.4b}$$

Here, $A^{\text{inc}}_{m,n}$ is the incident magnetic vector potential on the i^{th} wire, m direction, at $z = n$. Incident magnetic field in this case is the magnetic field generated by the other wires in the structure. The frequency-domain solution to 3.4 is explained in the next section.

3.2 Frequency Domain Solution

The frequency domain solution of (3.4) for the i^{th} conductor of length ℓ_i can be expressed in matrix form as [50]

$$\begin{bmatrix} V_i(0) \\ \\ I_i(0) \end{bmatrix} = \begin{bmatrix} \cos\beta\ell_i & jZ_0\sin\beta\ell_i \\ \\ j\dfrac{1}{Z_0}\sin\beta\ell_i & \cos\beta\ell_i \end{bmatrix} \begin{bmatrix} V_i(\ell_i) \\ \\ I_i(\ell_i) \end{bmatrix} + \int_0^{\ell_i} \begin{bmatrix} \cos\beta z' & jZ_0\sin\beta z' \\ \\ j\dfrac{1}{Z_0}\sin\beta z' & \cos\beta z' \end{bmatrix} \begin{bmatrix} V_F(z') \\ \\ I_F(z') \end{bmatrix} dz' \tag{3.5}$$

where,

$$\begin{bmatrix} V_F(z') \\ \\ I_F(z') \end{bmatrix} = \begin{bmatrix} j\omega A^{\text{inc}}_{z,z}\Big|_{x'=0}^{x'=h_i} \\ \\ \left(\dfrac{\partial A^{\text{inc}}_{z,z}}{\partial z} + \dfrac{\partial A^{\text{inc}}_{y,z}}{\partial y}\right)\Bigg|_{x'=0}^{x'=h_i} \end{bmatrix}.$$

Equation (3.5), theoretically, can be implemented on a set of wires directed arbitrarily at any direction, but is not likely to have a closed-form integral. However, for parallel wires of different lengths, (3.5) can be simplified further to have a closed-form given by

$$\begin{bmatrix} V_i(0) \\ \\ I_i(0) \end{bmatrix} = \begin{bmatrix} \cos\beta\ell_i & jZ_0\sin\beta\ell_i \\ \\ j\dfrac{1}{Z_0}\sin\beta\ell_i & \cos\beta\ell_i \end{bmatrix} \begin{bmatrix} V_i(\ell_i) \\ \\ I_i(\ell_i) \end{bmatrix} + \begin{bmatrix} \dfrac{j}{\sqrt{L_iC_i}}A^{\text{inc}}_{z,\ell_i}\sin(\beta\ell_i) \\ \\ \dfrac{1}{L_i}(A^{\text{inc}}_{z,\ell_i}\cos(\beta\ell_i) - A^{\text{inc}}_{z,0}) \end{bmatrix}_{x'=0}^{x'=h_i} . \quad (3.6)$$

Assuming a case of two parallel conductors (i and j) over a perfectly conducting ground, the incident magnetic vector potential on wire i at a length m, can be obtained using scattered field equation (2.8) and method of images as

$$A^{\text{inc}}_{z',m} = \frac{\mu}{4\pi}\int_{m-2h_j}^{m+2h_j}\left\{\left(\frac{e^{-j\beta R_{za}}}{R_{za}} - \frac{e^{-j\beta R_{zb}}}{R_{zb}}\right)I_j(z')\right\}dz' \quad (3.7a)$$

where,

$$R_{za} = \sqrt{(z-z')^2 + (x-h_j)^2 + d^2} \quad (3.7b)$$

$$R_{zb} = \sqrt{(z-z')^2 + (x+h_j)^2 + d^2}. \quad (3.7c)$$

In (3.7a), d is the distance between the two parallel conductors and $I_i(z')$ is the current on wire j at a length of z'. The exponential terms refer to the scalar Green's function related to the scattered field generated by I_i. As evident form (3.7), at $x' = 0$ (*i.e.* the ground level), the incident vector magnetic potential is zero. Graphical representation of (3.7b) and (3.7c) is given in Fig. 3.1.

The integral limits in (3.7a) are chosen such that the couplings are consistent with those of an infinitely long transmission line. Based on the decay of the scalar Green's function, it has been found that a current element can create a considerable coupling approximately up to a distance of $2h$ from it [15]. Using (3.6), $I_j(z')$ can be represented using terminal

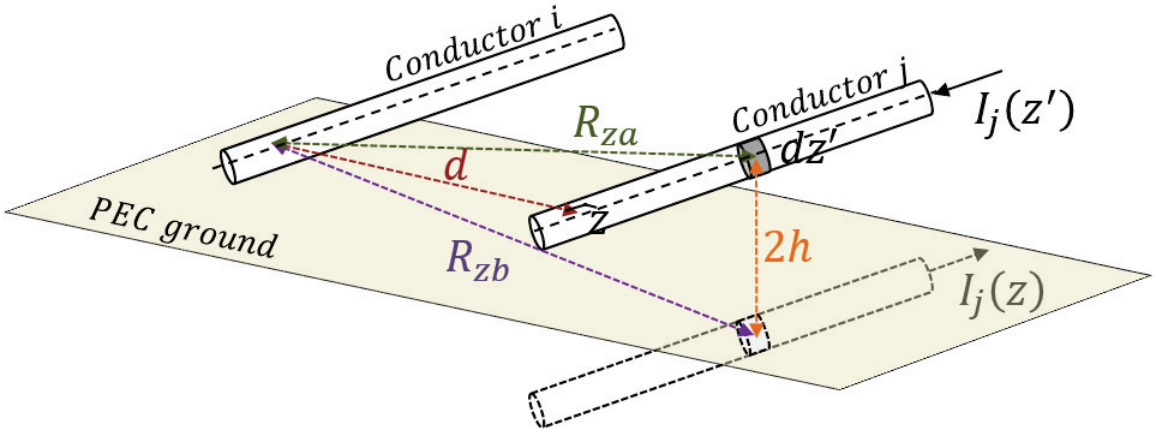

Fig. 3.1: Illustration of the method of images.

voltages and currents of wire 2 as

$$I_j(z') = j\frac{V_j(\ell_j)}{Z_{j,0}}\sin(\beta\,(\ell_j - z')) + I_j(\ell_j)\cos(\beta\,(\ell_j - z')) + \frac{1}{L_j}(A^{\text{inc}}_{z,\ell_j}\cos(\beta\ell_j) - A^{\text{inc}}_{z,z'}\cos(\beta z'). \tag{3.8}$$

In (3.8), instead of incorporating a weak coupling between conductors [50] *i.e.* considering only the first two terms on R.H.S of (3.8) we only neglect the last term. Therefore, we have included a stronger coupling between the conductors that results in more accurate results.

Using (3.6), (3.7), and (3.8) a final expression for wire i is in the following format given by

$$\begin{bmatrix} V_i(0) \\ I_i(0) \end{bmatrix} = \begin{bmatrix} S_{ii} \end{bmatrix} \begin{bmatrix} V_i(\ell_i) \\ I_i(\ell_i) \end{bmatrix} + \begin{bmatrix} M_{ij} \end{bmatrix} \begin{bmatrix} V_j(\ell_j) \\ I_j(\ell_j) \end{bmatrix}. \tag{3.9}$$

A similar expression can be obtained for wire j which can be combined with (3.9) to obtain a matrix equation in the format of

$$\begin{bmatrix} V_i(0) \\ V_j(0) \\ I_i(0) \\ I_j(0) \end{bmatrix} = \begin{bmatrix} \Phi \end{bmatrix} \begin{bmatrix} V_i(\ell_i) \\ V_j(\ell_j) \\ I_i(\ell_i) \\ I_j(\ell_j) \end{bmatrix} \tag{3.10}$$

which has the same structure of an MTL solution. Terminal constraints can be included using the same procedure as explained in [4] for classical MTL models. Once the frequency-domain solution is obtained, the time-domain solutions for various excitation waveforms can be obtained using the Inverse Fourier Transform (IFT).

3.3 Results and Discussion

The proposed method is used to model parallel conductors having different lengths and conductors placed electrically distant from each other above a PEC ground. Classical MTL method do not have the capability to model both these cases. Obtained results are compared with those from Numerical Electromagnetic Code (NEC). NEC is a thin-wire full-wave solver that numerically solves an electric field integral equation [16]. Since NEC solves for the frequency-domain current of each wire segment, time-domain terminal currents are obtained using the inverse Fourier transform method. It should also be noted that NEC doesn't produce the DC response and therefore for comparison, excitation waveforms without a DC component have to be used. However, NEC is widely used in the field of electromagnetics due to its accuracy and availability. The results obtained using the proposed model for three

cases of two lossless wires above PEC ground are presented in the following sections.

3.3.1 Parallel Conductors of Unequal Lengths

The purpose of this study was to understand whether the developed model can correctly represent the different travel times in wires due to variation of length in wire. Cases where the longer and shorter conductors are excited were implemented using the proposed method and results have been compared with those obtained from NEC. Figure 3.2 shows the modelled system of conductors where the longer wire is excited. The frequency responses of all terminal currents of this case are given in Figs. 3.3 - 3.6 along with those obtained from NEC.

As explained earlier since NEC does not produce the DC response, an excitation with a DC component could not be used for the comparison with time-domain results. Therefore, the derivative of a Gaussian waveform whose full width at half maximum (FWHM) is 250 MHz was used as V_s so that the wires are electrically close to each other at all frequencies. Figure 3.7 shows the frequency-domain and time-domain representations of the excitation waveform and it seen from fig.3.7a that for all dominant frequencies of the selected waveform the conductors are electrically close, which is 1.5 GHz. Figures 3.8 and 3.9 show the time-domain results of sending and receiving end currents respectively, compared with results obtained using NEC.

The same structure with the shorter wire excited, as shown in Fig. 3.10, is also analyzed. Figure 3.11 and 3.12 show the time-domain results for sending and receiving end currents of wire 1 and wire 2 compared with results obtained using NEC. As evident from the above two cases, the proposed SBC model has been able to correctly simulate the different travel times in conductors having different lengths.

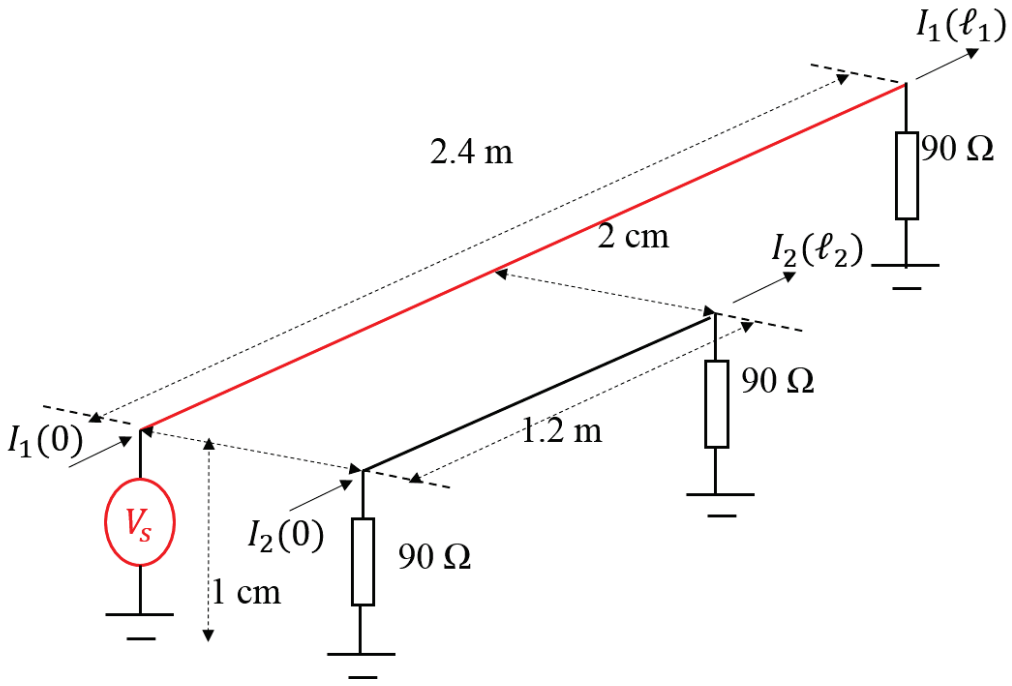

Fig. 3.2: System of conductors with the longer wire excited.

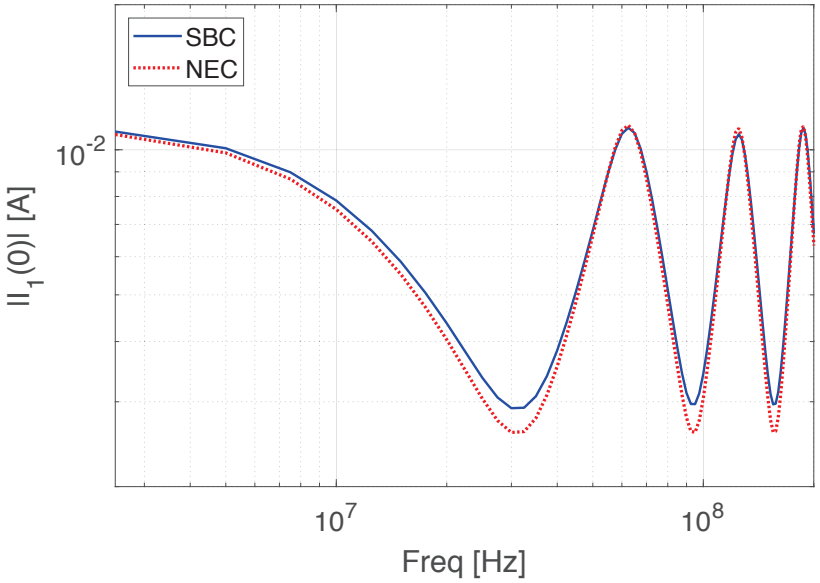

(a)

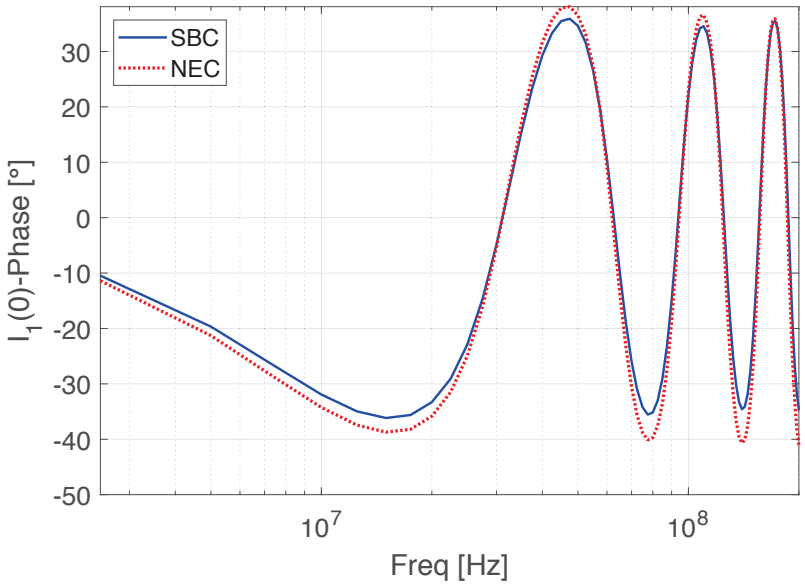

(b)

Fig. 3.3: (a) Magnitude and (b) phase of the frequency-domain response of the sending end current of the excited wire obtained using the proposed model (SBC) and NEC.

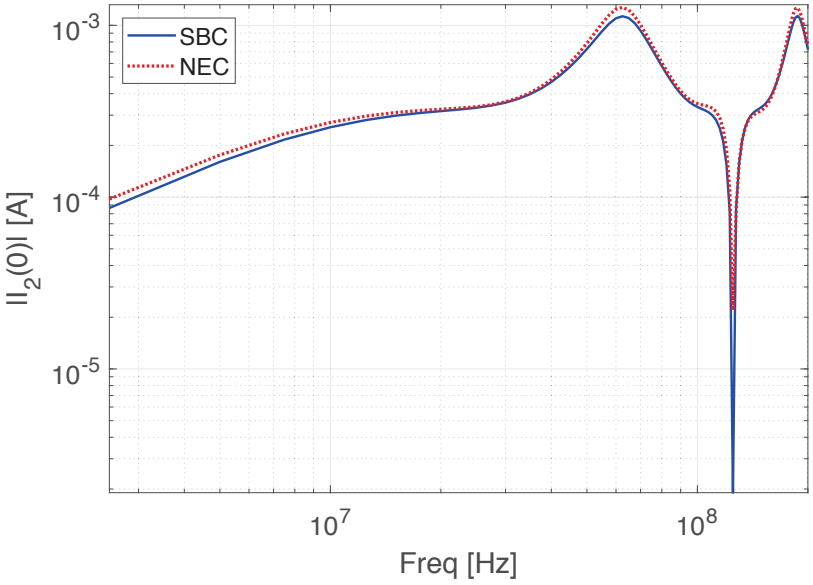

(a)

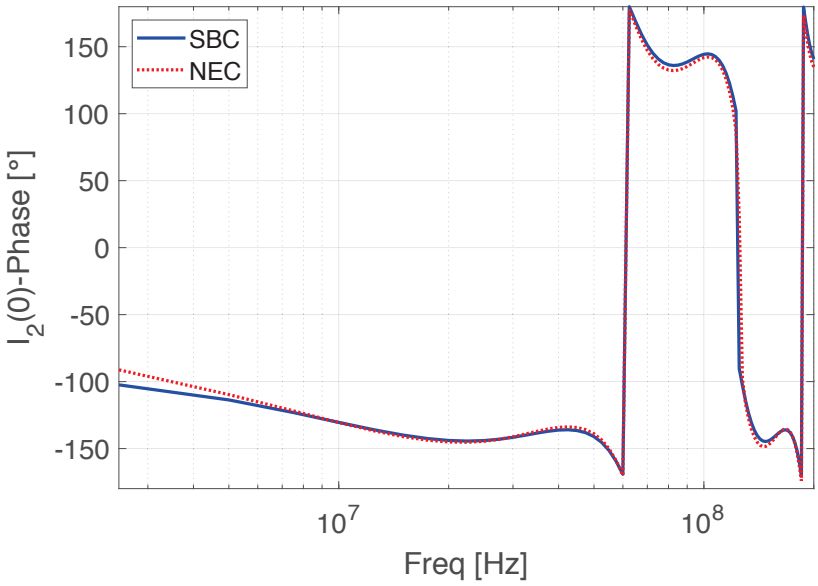

(b)

Fig. 3.4: (a) Magnitude and (b) phase of the frequency-domain response of the sending end current of the victim wire obtained using the proposed model (SBC) and NEC.

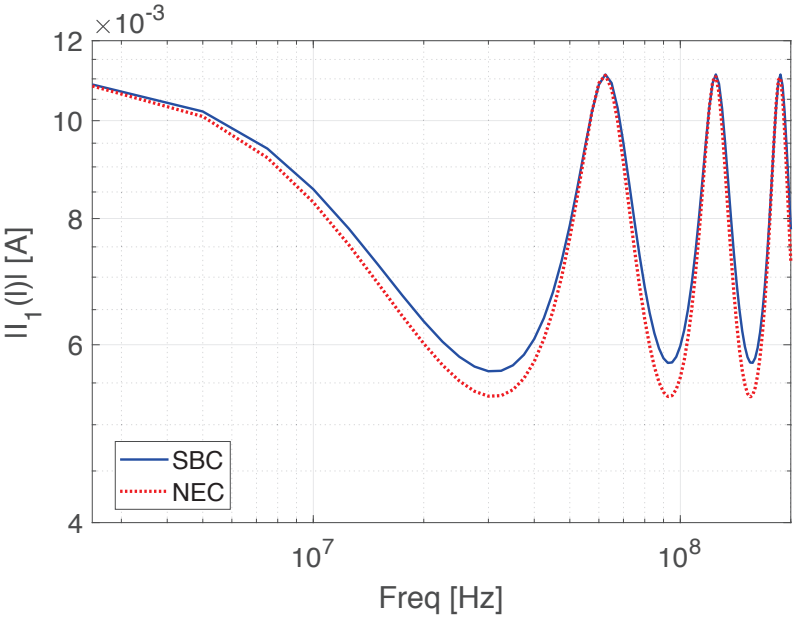

(a)

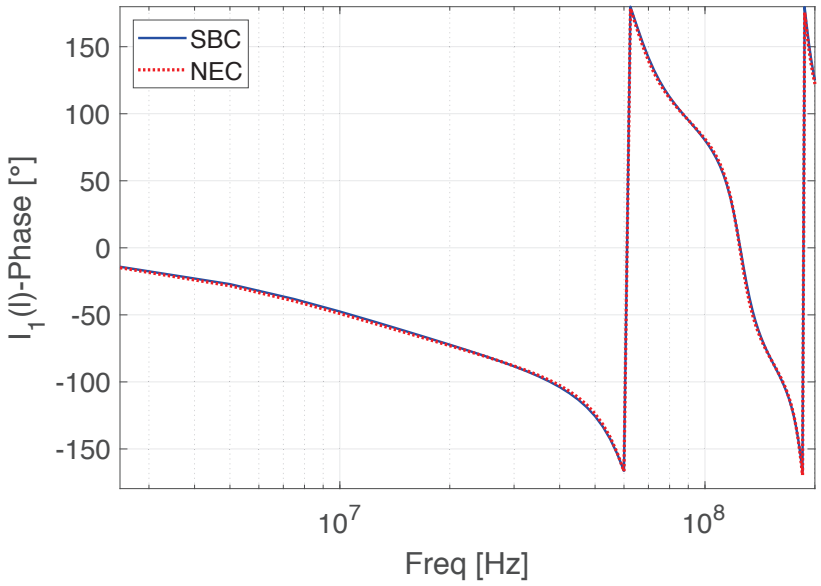

(b)

Fig. 3.5: (a) Magnitude and (b) phase of the frequency-domain response of the receiving end current of the excited wire obtained using the proposed model (SBC) and NEC.

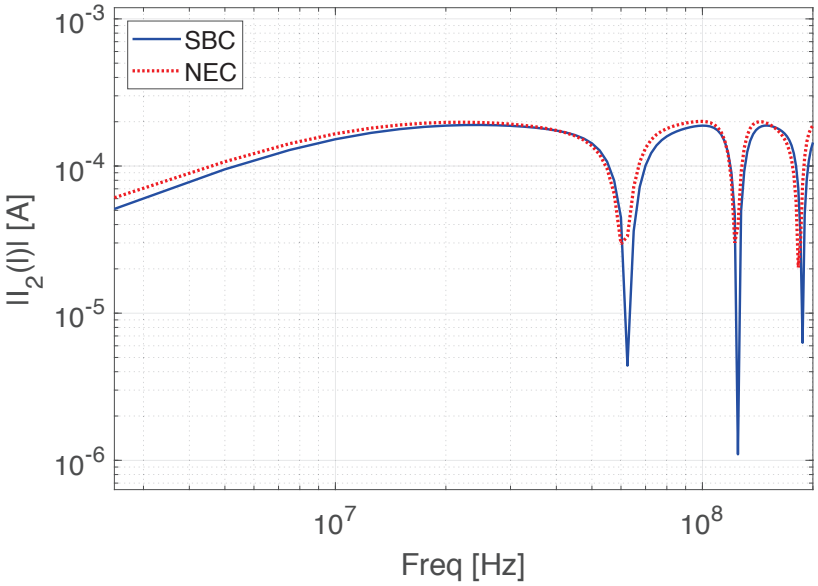

(a)

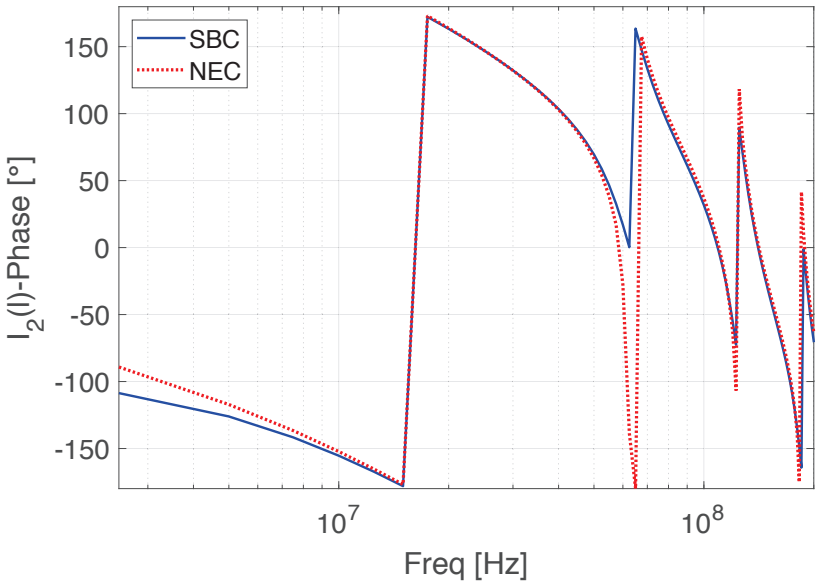

(b)

Fig. 3.6: (a) Magnitude and (b) phase of the frequency-domain response of the receiving end current of the victim wire obtained using the proposed model (SBC) and NEC.

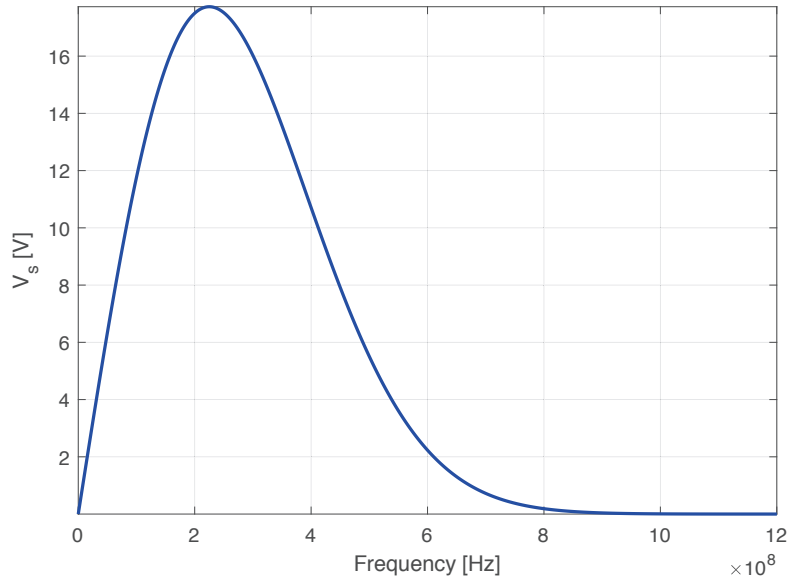

(a)

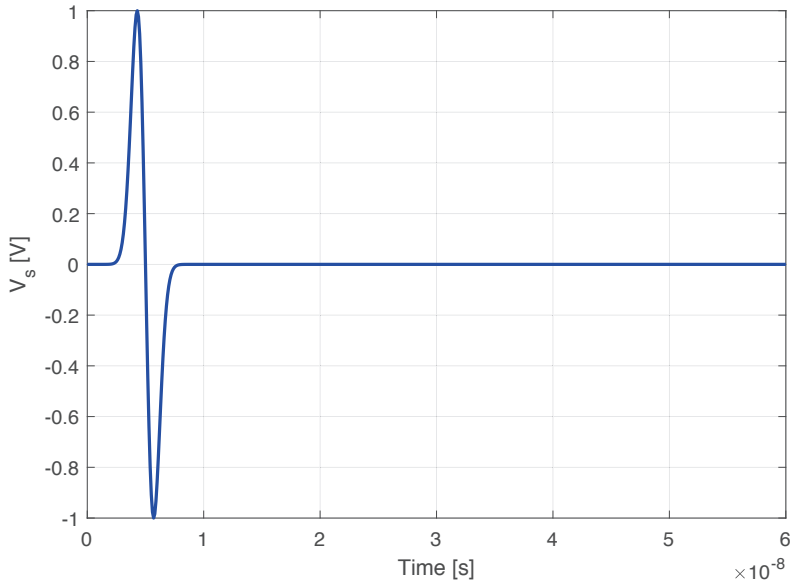

(b)

Fig. 3.7: (a) Frequency-domain and (b) time-domain representations of the excitation voltage (V_s) for time-domain analysis.

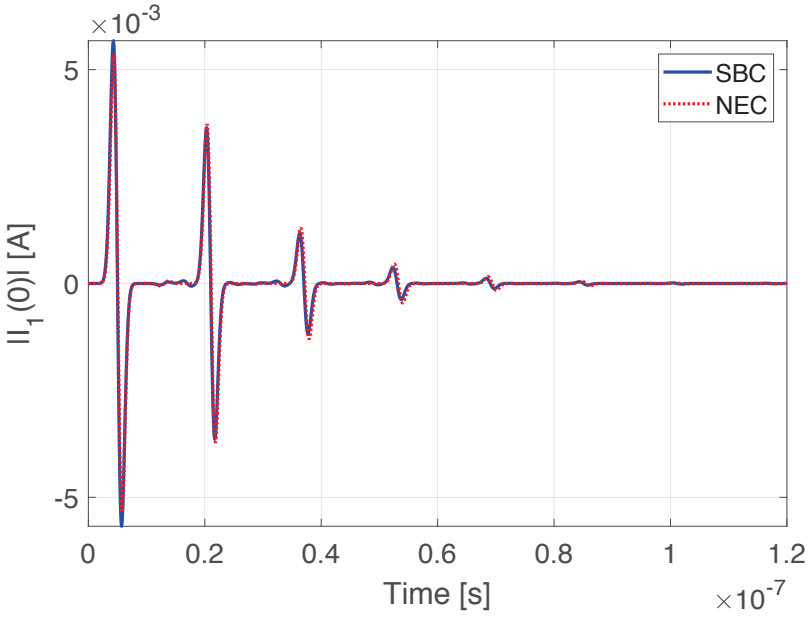

(a)

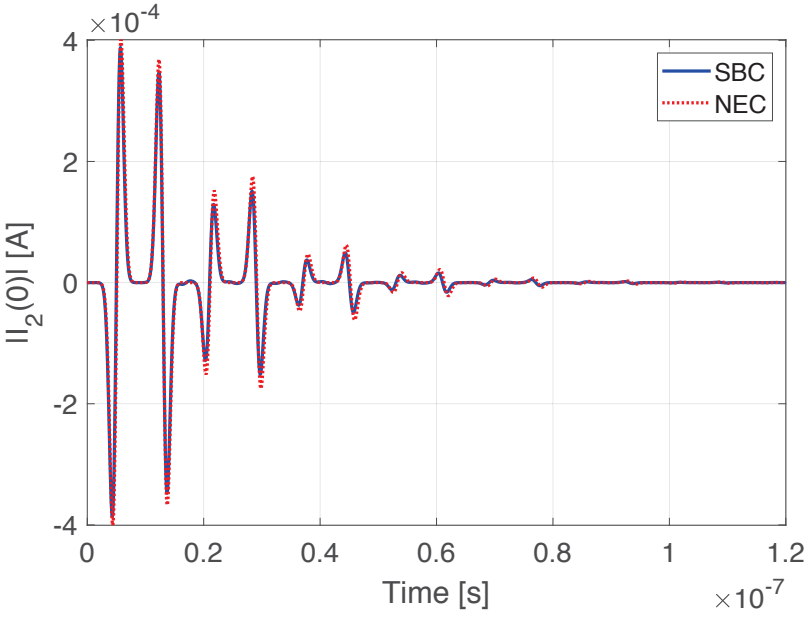

(b)

Fig. 3.8: Sending end currents of the (a) excited conductor and (b) victim conductor vs Time when the longer wire is excited obtained using the proposed model (SBC) and NEC.

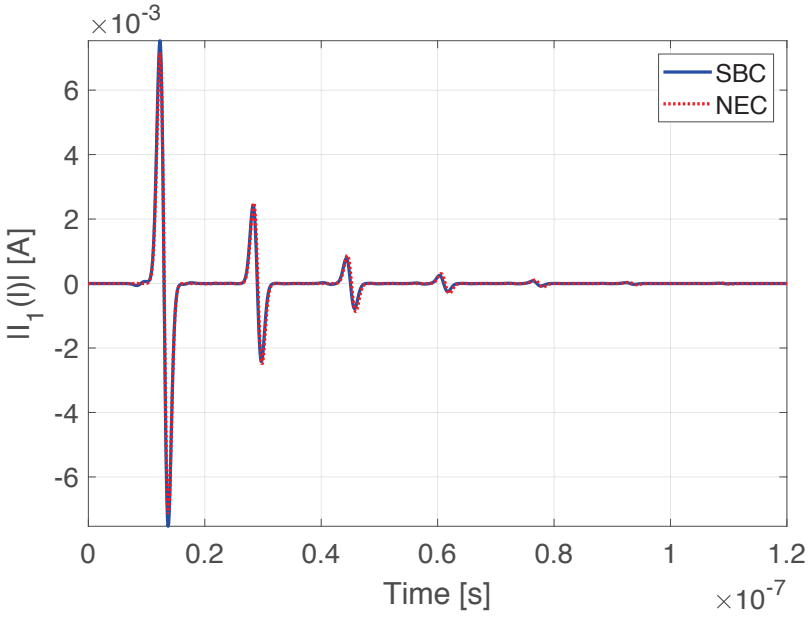

(a)

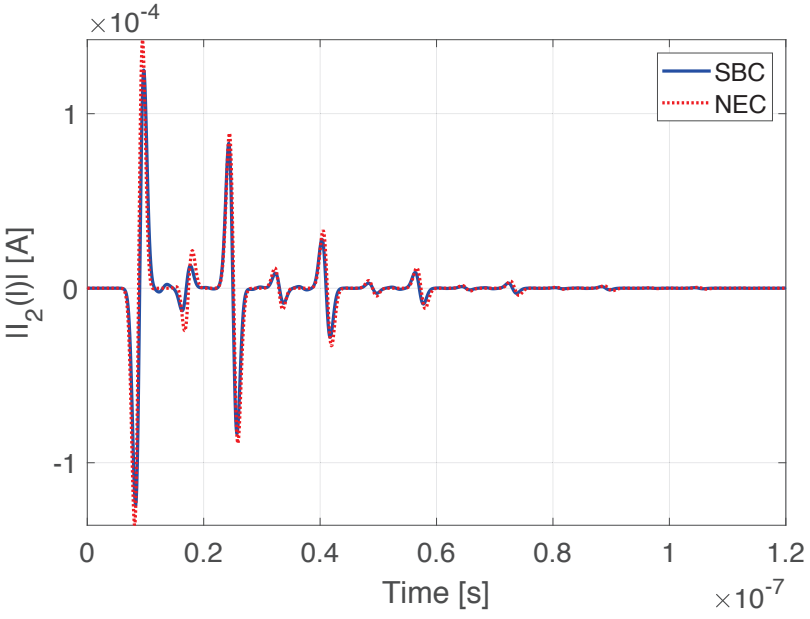

(b)

Fig. 3.9: Receiving end currents of the (a) excited conductor and (b) victim conductor vs Time when the longer wire is excited obtained using the proposed model (SBC) and NEC.

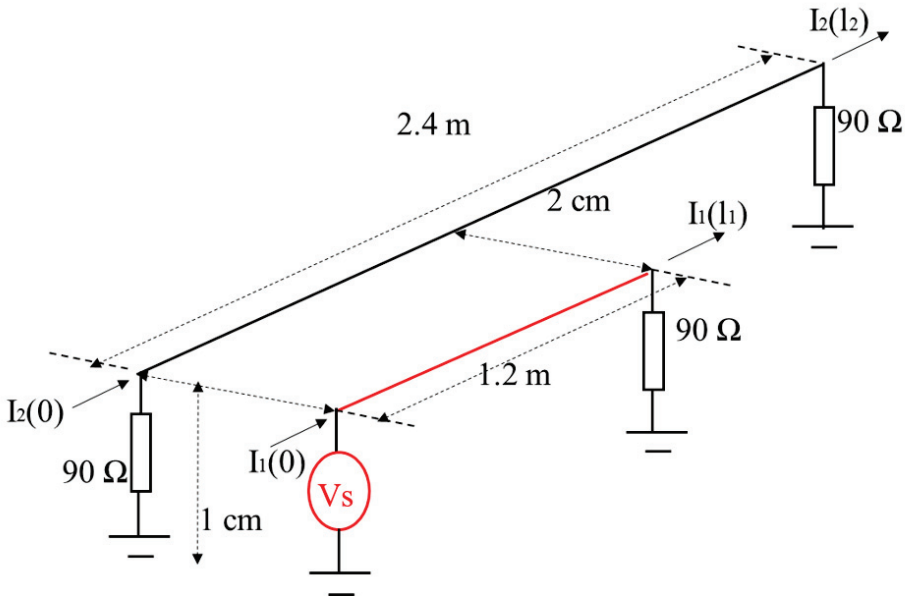

Fig. 3.10: System of conductors with shorter the wire excited.

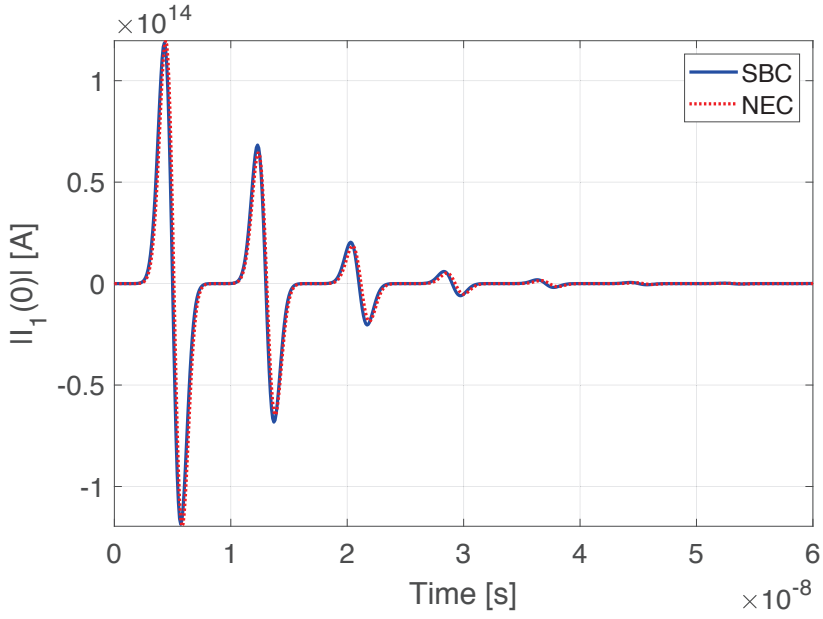

(a)

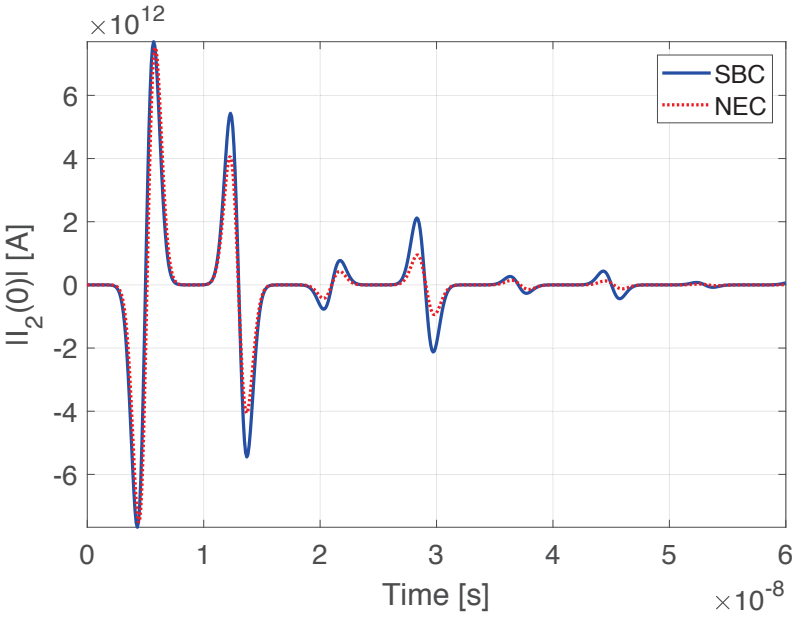

(b)

Fig. 3.11: Sending end currents of the (a) excited conductor and (b) victim conductor vs Time when the shorter wire is excited obtained using the proposed model (SBC) and NEC.

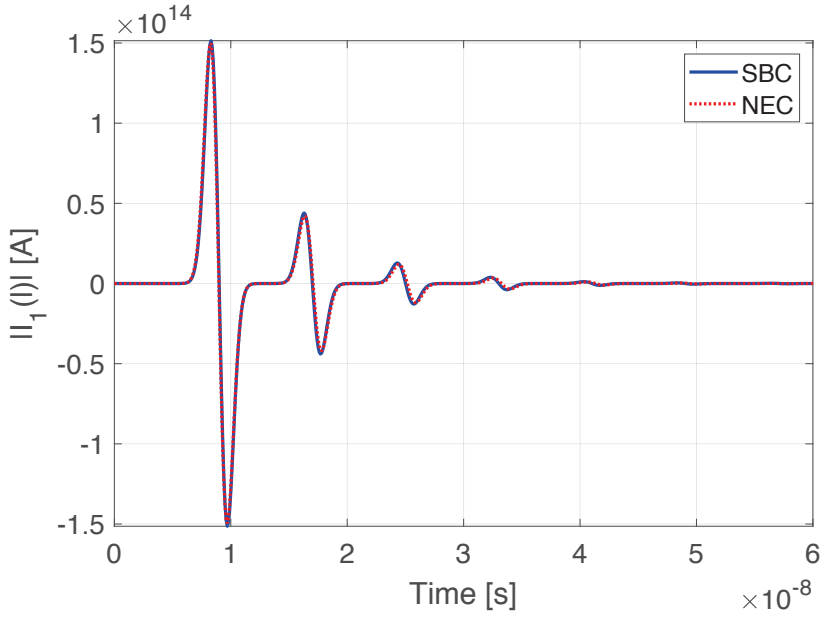

(a)

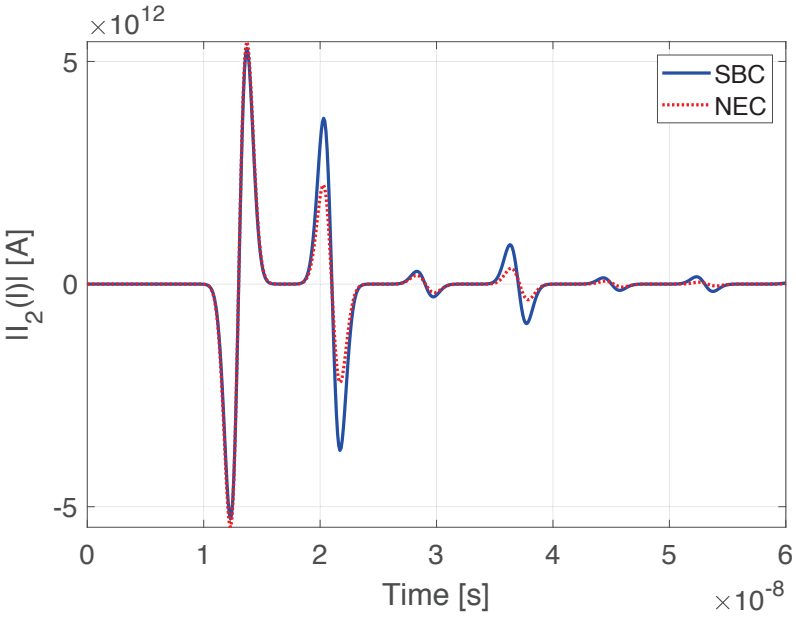

(b)

Fig. 3.12: Receiving end currents of the (a) excited conductor and (b) victim conductor vs Time when the shorter wire is excited obtained using the proposed model (SBC) and NEC.

3.3.2 Electrically Distant Parallel Conductors

Coupling between conductors in classical MTL models is assumed to be instantaneous and therefore these models are unable to show the time delay occurring when a wave travels through the medium from one conductor to the other one on the same cross-section. Therefore, classical MTL models are only valid when all cross sectional dimensions are small compared to the wavelengths of all frequencies of interest ($h_{max} < 0.1\lambda_{min}$). However, as (3.7a) depicts, the Green's function in the coupling terms of the proposed SBC model contains the delay occurring between conductors. Therefore the proposed model is capable of modelling conductors which are placed electrically far away from each other (but close to ground). It should also be noted that since the SBC model doesn't take radiation into account, it would not be valid for gap distances between wires above which higher order nodes start to propagate. However, there is no clear-cut gap distance for this to occur in open systems like two-wire lines, while for most of the closed systems such as coaxial cables it is usually around $0.5\lambda_{min}$ [4]. Incorporation of radiation in the formulae, as in the electric field integral equation used in NEC, requires the use of full-wave techniques to arrive at a solution, which is computationally cumbersome.

Figure 3.13 shows the system of conductors placed 50 cm apart from each other. A conventional MTL model will only be valid up to $f_0 = 60$ MHz for such a system (also MTL cannot model wires of different lengths). The frequency responses of the sending end currents obtained using the proposed model are shown in Figs. 3.14 and 3.15 along with those obtained using NEC. It can be seen that the proposed model is valid for frequencies well above the upper limit of classical MTL model.

The derivative of a Gaussian waveform with a FWHM of 100 MHz was used as the excitation waveform for the time-domain analysis which is shown in Fig. 3.16 in both the

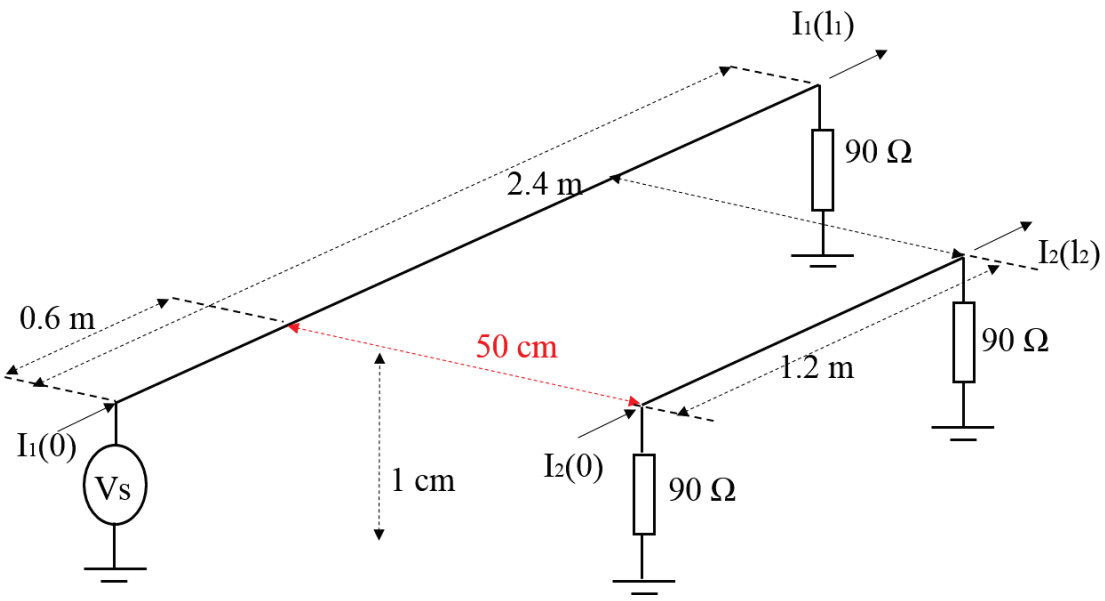

Fig. 3.13: System of conductors electrically distant for frequencies above 60 MHz.

frequency and time domains. As fig. 3.16a suggests, the excitation waveform has dominant frequencies (dominant frequencies were taken as frequencies with more than 50% of the highest magnitude) up to approximately 150 MHz.

Figures 3.17 and 3.18 show the sending end currents of the system respectively in the time-domain. The proposed approach has been able to model the time-delay that occurs during the coupling between wires placed electrically far away from each conductor.

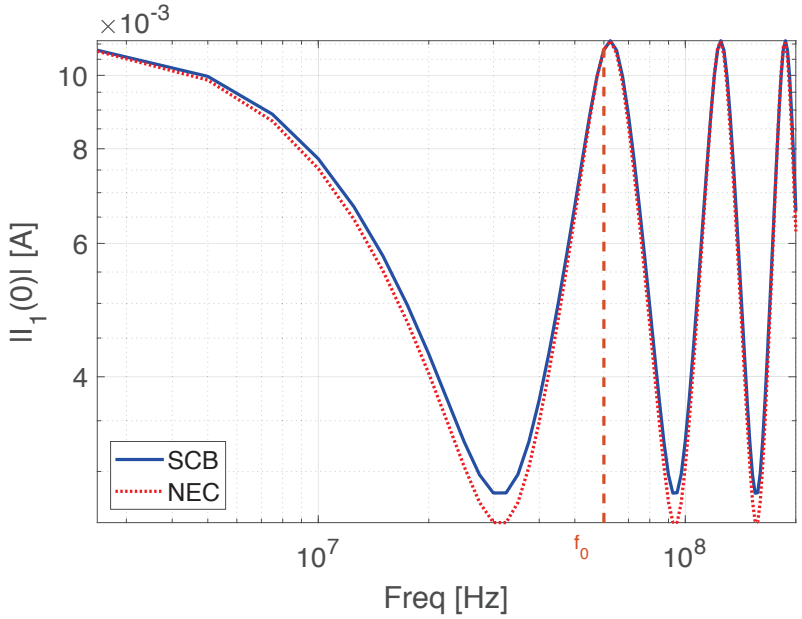

(a)

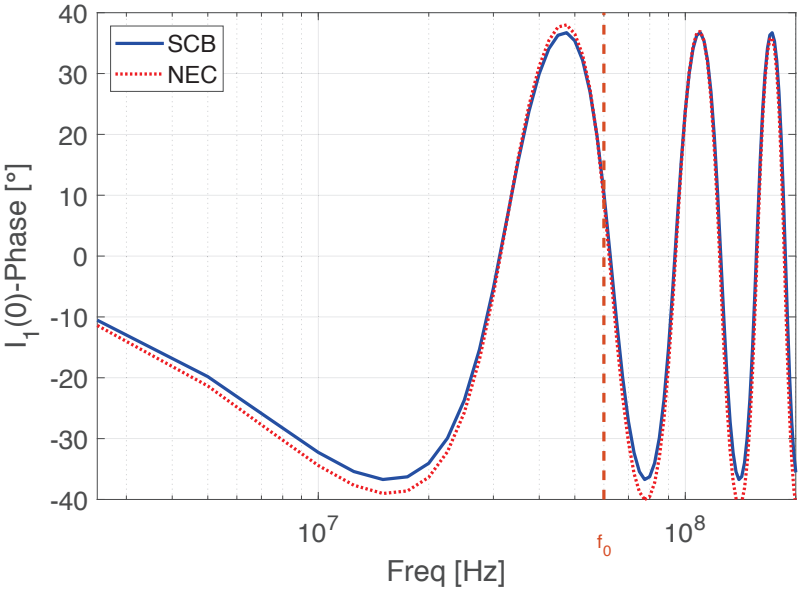

(b)

Fig. 3.14: (a) Magnitude and (b) phase of the sending end frequency-response of the excited wire obtained using the proposed model (SBC) and NEC.

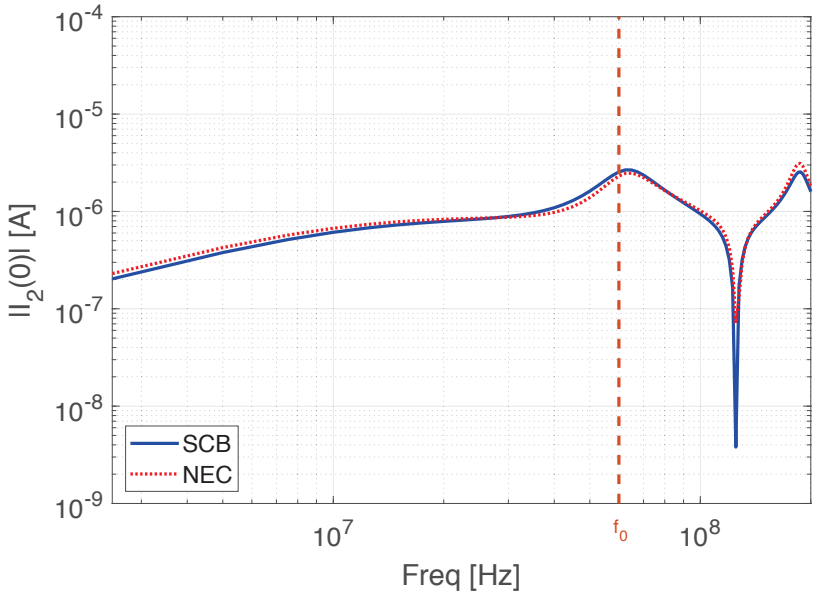

(a)

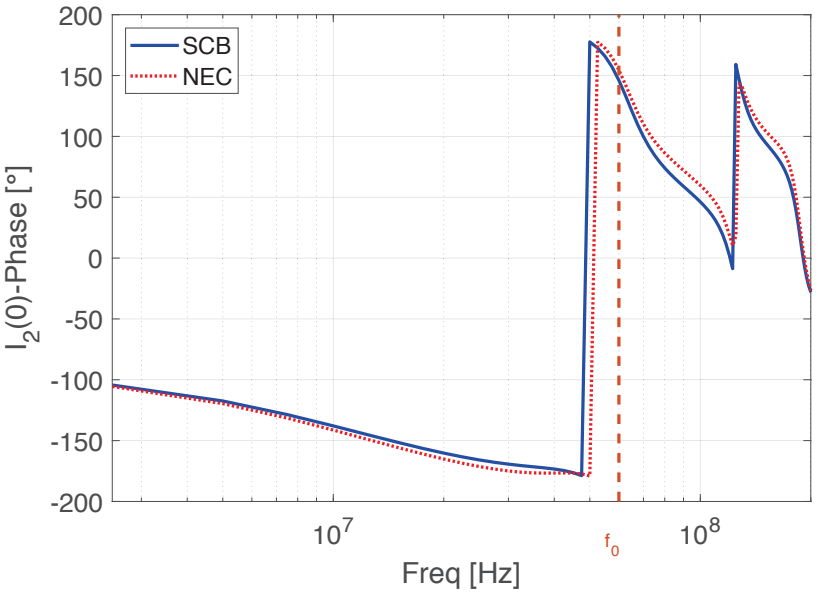

(b)

Fig. 3.15: (a) Magnitude and (b) phase of the sending end frequency-response of the victim wire obtained using the proposed model (SBC) and NEC.

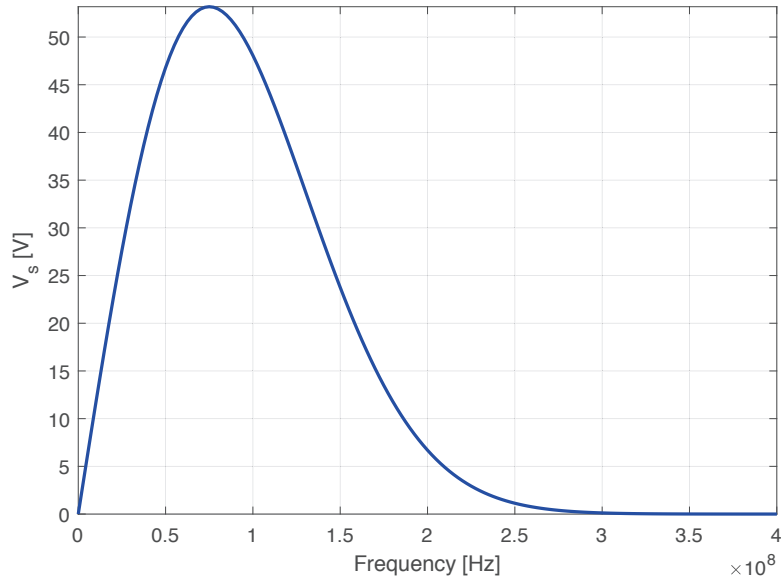

(a)

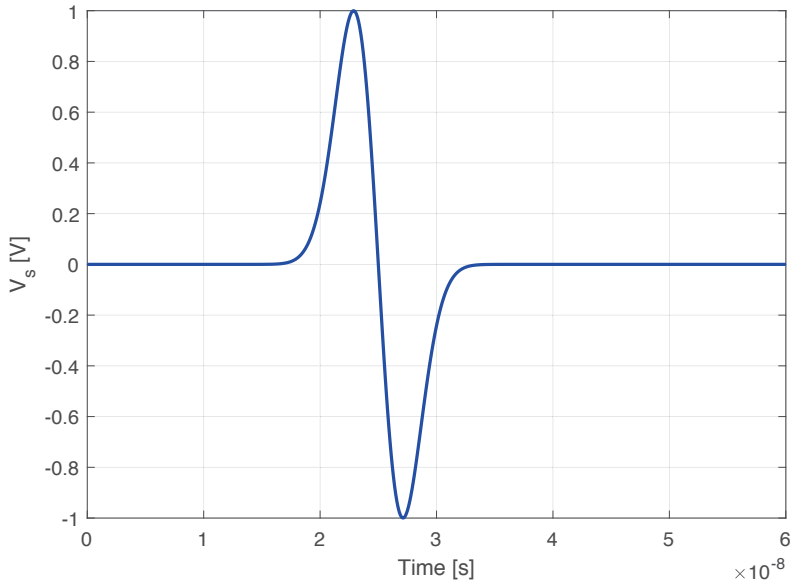

(b)

Fig. 3.16: (a) Frequency-domain and (b) time-domain representations of the excitation voltage (V_s) for time-domain analysis.

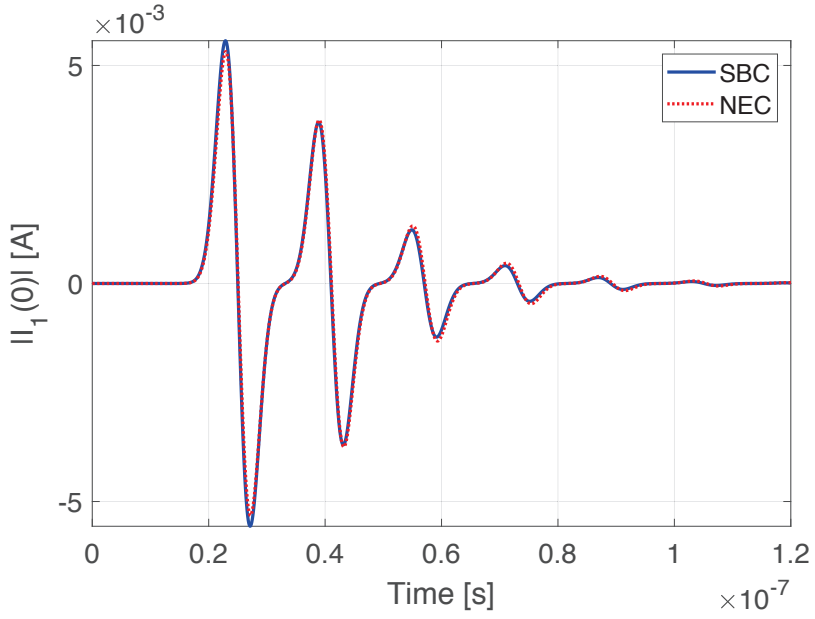

(a)

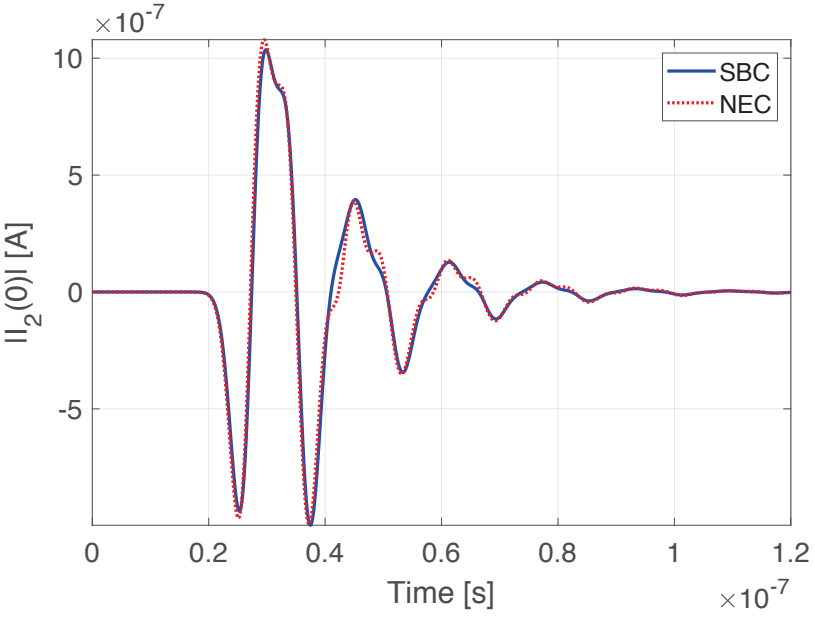

(b)

Fig. 3.17: Sending end currents of the (a) excited conductor and (b) victim conductor vs Time, obtained using the proposed model (SBC) and NEC.

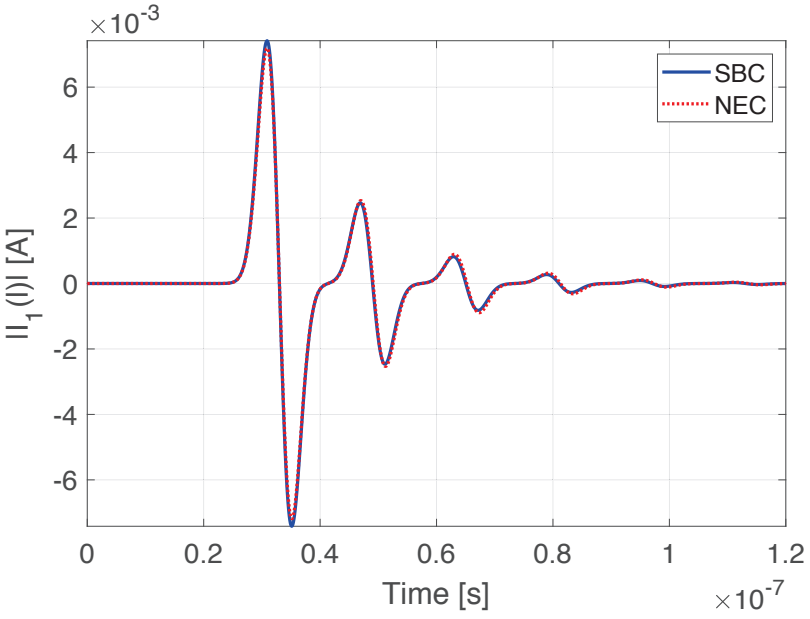

(a)

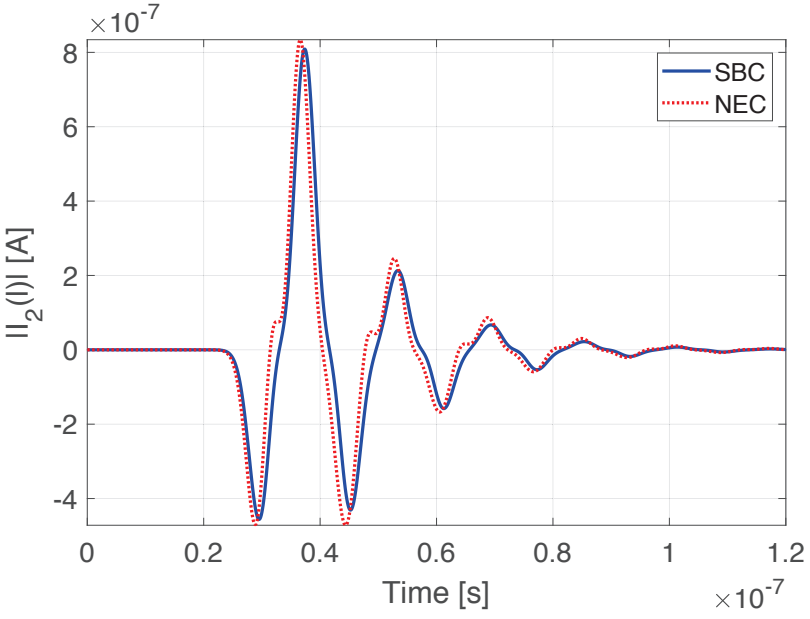

(b)

Fig. 3.18: Receiving end currents of the (a) excited conductor and (b) victim conductor vs Time, obtained using the proposed model (SBC) and NEC.

3.4 Summary

In this chapter an enhancement to the classical MTL model based on scattering theory has been developed. In the developed scattering based coupling (SBC) model, the self coupling of each conductor is modelled using classical MTL parameters, while the mutual coupling between conductors is modelled using electromagnetic scattering theory. Compared to classical MTL models the developed closed-form model has the ability to model parallel conductors of different lengths, and conductors placed electrically distant from each other, but close to ground, in both frequency and time domains. Applicability of the SBC model is currently limited to lossless, thin-wire structures. The developed model has been compared with a full-wave, thin-wire solver.

Chapter 4

Scattered Field Transmission Line Model

In this chapter the development of a time-domain model for transmission line crossings and bends in finite-length conductors is presented. The exciting electromagnetic field is first formulated using the scattering equations and then simplified into closed-forms based on the geometrical and frequency characteristics of transmission lines. The simplified equations are solved using a FDTD algorithm. Results obtained using the proposed model are presented along with those obtained using a full-wave finite-element solver.

A scattered electric field produced by vector and scalar potentials can be represented as [15]

$$\boldsymbol{E}^s = -j\omega\boldsymbol{A} - \nabla\Phi \tag{4.1}$$

with

$$\boldsymbol{A}(\boldsymbol{r}) = \frac{\mu}{4\pi}\int_0^\ell I(z')\hat{a}_z g(\boldsymbol{r},\boldsymbol{r}')\,dz'$$

and,

$$\Phi(\boldsymbol{r}) = \frac{1}{4\pi\varepsilon}\int_0^\ell \rho(z')g(\boldsymbol{r},\boldsymbol{r}')\,dz'$$

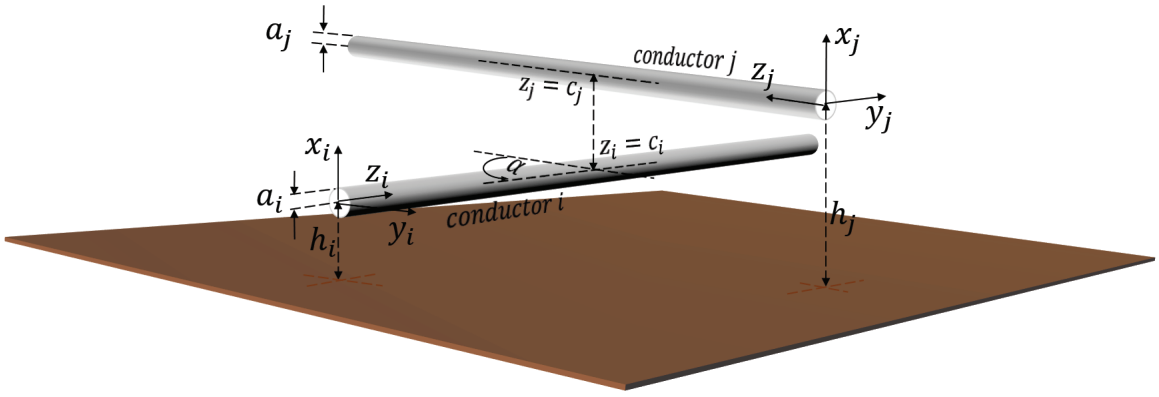

Fig. 4.1: Cylindrical conductors crossing each other and their local coordinate systems.

where z' is the length variable along the axis of wire, $\boldsymbol{r} = x\hat{a}_x + y\hat{a}_y + z\hat{a}_z$ is the position vector of the observation point and $\boldsymbol{r}'$ is the position vector of the source. $I(z')$ and $\rho(z')$ are the current and charge density along the wire. It was explained in chapter 3 that the Green's functions, $g(\boldsymbol{r}, \boldsymbol{r}')$ of the thin-wire problem has a value of zero at the ground level since the distances from the source and image currents are equal at the ground level. Therefore $\boldsymbol{A}$ and Φ at $h = 0$ will be omitted in the formulation here onwards.

4.1 Scattering Model for a Transmission Line Crossing

Since classical MTL models are unable to simulate a crossing of conductors as shown in Fig. 4.1, the proposed approach is to model it using scattered fields and simply into a transmission line like form. Since the objective of this on-going work is to include SFTL model in EMT-type simulators, it has been implemented using an FDTD algorithm.

4.1.1 Derivation of Scattering Equations for Crossed Wires

For the structure shown in Fig. 4.1, under thin-wire approximation, the scattered magnetic vector potential along z direction and scalar potential, on conductor i can be expressed respectively as [15]

$$\begin{aligned}\boldsymbol{A}_{z_i}(z_i) =& \frac{\mu}{4\pi}\int_0^{\ell_i} g\left(z_i, z_i{}'\right) I_i(z_i{}')dz_i{}' \\ &+ \cos\alpha\frac{\mu}{4\pi}\int_0^{\ell_j} g\left(z_i, z_j, \alpha\right) I_j(z_j)dz_j\end{aligned} \tag{4.2a}$$

and,

$$\begin{aligned}\Phi(z_i) =& \frac{1}{4\pi\varepsilon}\int_0^{\ell_i} g\left(z_i, z_i{}'\right) \rho_i(z_i{}')dz_i{}' \\ &+ \frac{1}{4\pi\varepsilon}\int_0^{\ell_j} g\left(z_i, z_j, \alpha\right) \rho_j(z_j)dz_j.\end{aligned} \tag{4.2b}$$

In (4.2), ℓ_i and ℓ_j are the lengths of conductors i and j. I_i and I_j are the currents and ρ_i and ρ_j are the electric charge densities at a field point on the surface of the wires i and j respectively. α is the crossing angle and g is the Green's function related to a scattered field generated by a straight, cylindrical, current carrying conductor, which can be obtained using the method of images as given by [30]

$$g(z_i, z_i{}') = \frac{e^{-j\beta\sqrt{(z_i{}'-z_i)^2+a_i^2}}}{\sqrt{(z_i{}'-z_i)^2+a_i^2}} - \frac{e^{-j\beta\sqrt{(z_i{}'-z_i)^2+(2h_i)^2}}}{\sqrt{(z_i{}'-z_i)^2+(2h_i)^2}} \tag{4.3a}$$

and,

$$g(z_i, z_j, \alpha) = \frac{e^{-j\beta\sqrt{((c_i-z_i)\sin\alpha)^2+((c_j-z_j)+(c_i-z_i)\cos\alpha)^2+(h_i-h_j)^2}}}{\sqrt{((c_i-z_i)\sin\alpha)^2+((c_j-z_j)+(c_i-z_i)\cos\alpha)^2+(h_i-h_j)^2}} - \frac{e^{-j\beta\sqrt{((c_i-z_i)\sin\alpha)^2+((c_j-z_j)+(c_i-z_i)\cos\alpha)^2+(h_i+h_j)^2}}}{\sqrt{((c_i-z_i)\sin\alpha)^2+((c_j-z_j)+(c_i-z_i)\cos\alpha)^2+(h_i+h_j)^2}}. \tag{4.3b}$$

As mentioned in the previous sections, the field point (point of observation) is assumed to be on the wire surface while the source point is assumed to be on the axis, in order to avoid the singularity that can occur in the Green's functions at $z_i{}' = z_i$. The boundary condition on the surface of the wire would be that, the scattered electric field is tangential to the z direction. Assuming that there are no incident fields, this gives [15]

$$\hat{a_z} \cdot \boldsymbol{E}^s = 0 \tag{4.4}$$

where $\boldsymbol{E}^s$ is the scattered electric field Using this (4.1) can be rewritten as

$$\frac{\mathrm{d}\Phi}{\mathrm{d}z_i} = -j\omega A_{z_i}. \tag{4.5}$$

Under the thin-wire approximation it can be assumed that the direction of the current is only along the z axis which gives

$$A_x = A_y = 0. \tag{4.6}$$

Since the scattered voltage is defined as [15],

$$V(z_i) = -\int_0^{h_i} E_x^s dx \tag{4.7}$$

(4.6) and (4.1) can be used to rewrite (4.7) as,

$$V(z_i) = \Phi(z_i). \tag{4.8}$$

Substituting (4.8) into (4.5) gives,

$$\frac{\mathrm{d}V(z_i)}{\mathrm{d}z_i} = -j\omega A_{z_i}. \tag{4.9}$$

Using (4.2a) and (4.9) a transmission line like expression can be obtained as

$$\begin{aligned}\frac{\mathrm{d}V(z_i)}{\mathrm{d}z_i} = &-j\omega\frac{\mu}{4\pi}\int_0^{\ell_i} g\left(z_i, {z_i}'\right) I_i({z_i}')d{z_i}'\Big|_{y_i=h_i} \\ &- j\omega\frac{\mu}{4\pi}\cos\alpha\int_0^{\ell_j} g\left(z_i, z_j, \alpha\right) I_j(z_j)dz_j\Big|_{y_i=h_i}.\end{aligned} \tag{4.10}$$

Also, the electric charge density ρ can be expressed using the conductor current as given in the continuity equation as [15]

$$\rho_i(z_i) = -\frac{1}{j\omega}\frac{\mathrm{d}I(z_i)}{\mathrm{d}z_i}. \tag{4.11}$$

Equation (4.11) can be substituted into (4.2b) and re-arranged to obtain a second transmission line like expression as,

$$\begin{aligned}V(z_i) = &-\frac{1}{4\pi\varepsilon}\int_0^{\ell_i} g\left(z_i, {z_i}'\right)\frac{1}{j\omega}\frac{\mathrm{d}I({z_i}')}{\mathrm{d}z_i}d{z_i}'\Big|_{y_i=h_i} \\ &- \frac{1}{4\pi\varepsilon}\int_0^{\ell_j} g\left(z_i, z_j, \alpha\right)\frac{1}{j\omega}\frac{\mathrm{d}I(z_j)}{\mathrm{d}z_j}dz_j\Big|_{y_i=h_i}.\end{aligned} \tag{4.12}$$

The integral terms in (4.10) and (4.12) do not have analytical solutions in their raw form and therefore need to be simplified further before implementing on a FDTD algorithm.

4.1.2 Closed-form Equations Based on Structural Dimensions and Frequency

For the case of power transmission lines, as well as other situations where the classical MTL theory can be applied, the maximum cross-sectional dimension of the structure is very small compared to the minimum wavelength considered in the analysis. Therefore, based on the assumption that $h_{max} << \lambda$, the integral terms in (4.10) and (4.12) can be simplified that yields [15]

$$\begin{aligned}\int g(z,z')I(z')dz' &= \int \left(\frac{e^{-j\beta R_s}}{R_s} - \frac{e^{-j\beta R_i}}{R_i}\right) I(z')dz' \\ &= \int \left(\frac{1}{R_s} - \frac{1}{R_i}\right) dz' I(z).\end{aligned} \tag{4.13}$$

In this equation, R_s and R_i are respectively, the distances to point z from the current element and image current element at z', which are also the square root terms in (4.3). The simplified integral in (4.13) has an analytical solution. Assuming the analytical solutions for the integrals are represented as $\xi(z)$, (4.10) and (4.12) can be rewritten as,

$$\frac{\mathrm{d}V(z_i)}{\mathrm{d}z_i} = -j\omega\frac{\mu}{4\pi}\xi_{ii}(z_i)I_i(z_i) - j\omega\frac{\mu}{4\pi}\cos\alpha\xi_{ij}(z_i)I_j(z_j) \tag{4.14a}$$

and,

$$V(z_i) = -\frac{1}{j\omega 4\pi\varepsilon}\xi_{ii}(z_i)\frac{\mathrm{d}I_i(z_i)}{\mathrm{d}z_i} - \frac{1}{j\omega 4\pi\varepsilon}\xi_{ij}(z_i)\frac{\mathrm{d}I_j(z_j)}{\mathrm{d}z_j}. \tag{4.14b}$$

Similarly for conductor j electromagnetic field equations can be derived as,

$$\frac{\mathrm{d}V(z_j)}{\mathrm{d}z_j} = -j\omega\frac{\mu}{4\pi}\cos\alpha\xi_{ji}(z_j)I_i(z_i) - j\omega\frac{\mu}{4\pi}\xi_{jj}(z_j)I_j(z_j) \tag{4.15a}$$

and,

$$V(z_j) = -\frac{1}{j\omega 4\pi\varepsilon}\xi_{ji}(z_j)\frac{\mathrm{d}I_i(z_i)}{\mathrm{d}z_i} - \frac{1}{j\omega 4\pi\varepsilon}\xi_{jj}(z_j)\frac{\mathrm{d}I_j(z_j)}{\mathrm{d}z_j}. \tag{4.15b}$$

The analytical solutions of each integral of (4.14) and (4.15) are given by [52]

$$\begin{aligned}\xi_{ii}(z_i) = &\left[\sinh^{-1}\left(\frac{\ell_i - z_i}{a_i}\right) - \sinh^{-1}\left(\frac{-z_i}{a_i}\right)\right] \\ &- \left[\sinh^{-1}\left(\frac{\ell_i - z_i}{2h_i}\right) - \sinh^{-1}\left(\frac{-z_i}{2h_i}\right)\right]\end{aligned} \tag{4.16a}$$

$$\begin{aligned}\xi_{ij}(z_i) = &\left[\sinh^{-1}\left(\frac{\ell_j - c_j + (c_i - z_i)}{\sqrt{\left((c_i - z_i)\sin(\alpha)\right)^2 + (h_i - h_j)^2}}\right)\right. \\ &\left. - \sinh^{-1}\left(\frac{-c_j + (c_i - z_i)}{\sqrt{\left((c_i - z_i)\sin(\alpha)\right)^2 + (h_i - h_j)^2}}\right)\right] \\ &- \left[\sinh^{-1}\left(\frac{\ell_j - c_j + (c_i - z_i)}{\sqrt{\left((c_i - z_i)\sin(\alpha)\right)^2 + (h_i + h_j)^2}}\right)\right. \\ &\left. - \sinh^{-1}\left(\frac{-c_j + (c_i - z_i)}{\sqrt{\left((c_i - z_i)\sin(\alpha)\right)^2 + (h_i + h_j)^2}}\right)\right]\end{aligned} \tag{4.16b}$$

$$\begin{aligned}\xi_{ji}(z_j) = &\left[\sinh^{-1}\left(\frac{\ell_i - c_i + (c_j - z_j)}{\sqrt{\left((c_j - z_j)\sin(\alpha)\right)^2 + (h_i - h_j)^2}}\right)\right. \\ &\left. - \sinh^{-1}\left(\frac{-c_j + (c_j - z_j)}{\sqrt{\left((c_j - z_j)\sin(\alpha)\right)^2 + (h_i - h_j)^2}}\right)\right] \\ - &\left[\sinh^{-1}\left(\frac{\ell_i - c_i + (c_j - z_j)}{\sqrt{\left((c_j - z_j)\sin(\alpha)\right)^2 + (h_i + h_j)^2}}\right)\right. \\ &\left. - \sinh^{-1}\left(\frac{-c_i + (c_j - z_j)}{\sqrt{\left((c_j - z_j)\sin(\alpha)\right)^2 + (h_i + h_j)^2}}\right)\right]\end{aligned} \tag{4.16c}$$

and

$$\begin{aligned}\xi_{jj}(z_j) = &\left[\sinh^{-1}\left(\frac{\ell_j - z_j}{a_j}\right) - \sinh^{-1}\left(\frac{-z_j}{a_j}\right)\right] \\ &- \left[\sinh^{-1}\left(\frac{\ell_j - z_j}{2h_j}\right) - \sinh^{-1}\left(\frac{-z_j}{2h_j}\right)\right].\end{aligned} \tag{4.16d}$$

After rearranging, (4.14) and (4.15) can be expressed in a matrix form as,

$$\frac{\mathrm{d}}{\mathrm{d}z}\begin{bmatrix}\boldsymbol{V}(z, j\omega) \\ \boldsymbol{I}(z, j\omega)\end{bmatrix} = -j\omega\begin{bmatrix}\boldsymbol{L}(z) & 0 \\ 0 & \boldsymbol{C}(z)\end{bmatrix}\begin{bmatrix}\boldsymbol{V}(z, j\omega) \\ \boldsymbol{I}(z, j\omega)\end{bmatrix} \tag{4.17a}$$

where,

$$\boldsymbol{L}(z) = \frac{\mu}{4\pi}\begin{bmatrix}\xi_{ii}(z) & \cos\alpha\xi_{ij}(z) \\ \cos\alpha\xi_{ji}(z) & \xi_{jj}(z)\end{bmatrix}$$

$$\boldsymbol{C}(z) = 4\pi\varepsilon \begin{bmatrix} \dfrac{\xi_{jj}(z)}{\xi_{ii}(z)\xi_{jj}(z) - \xi_{ij}(z)\xi_{ji}(z)} & \dfrac{-\xi_{ij}(z)}{\xi_{ii}(z)\xi_{jj}(z) - \xi_{ij}(z)\xi_{ji}(z)} \\ \dfrac{-\xi_{ji}(z)}{\xi_{ii}(z)\xi_{jj}(z) - \xi_{ij}(z)\xi_{ji}(z)} & \dfrac{\xi_{ii}(z)}{\xi_{ii}(z)\xi_{jj}(z) - \xi_{ij}(z)\xi_{ji}(z)} \end{bmatrix}.$$

The reason for using a common z instead of z_i and z_j will be explained in the next section. Since $\boldsymbol{L}$ and $\boldsymbol{C}$ are frequency independent, (4.17a) can be converted into time-domain conveniently as,

$$\frac{\mathrm{d}}{\mathrm{d}z}\begin{bmatrix} \boldsymbol{V}(z,t) \\ \boldsymbol{I}(z,t) \end{bmatrix} = -\frac{\mathrm{d}}{\mathrm{d}t}\begin{bmatrix} \boldsymbol{L}(z) & 0 \\ 0 & \boldsymbol{C}(z) \end{bmatrix}\begin{bmatrix} \boldsymbol{V}(z,t) \\ \boldsymbol{I}(z,t) \end{bmatrix}. \tag{4.18}$$

Equation (4.18) along with terminal constraints can be solved using a single dimensional FDTD algorithm [4] for each time step. The terminal constraints could be the circuitry attached to the end of the wires or terminal voltage and current at each time-step of another transmission line connected to the particular end.

4.1.3 FDTD algorithm for solving the proposed model

Finite-difference time-domain technique explained in [4] is used to solve the developed SFTL model. For lossless lines descretized into NDZ segments as shown in Fig. 4.2, the voltage vectors of the NDZ + 1 nodes and the current vectors of the NDZ segments can be obtained using [4]

$$\boldsymbol{V}_1^{n+1} = \left[\frac{\Delta z}{\Delta t}\boldsymbol{R}_S\boldsymbol{C} + \mathbf{1}_n\right]^{-1}\left\{\left[\frac{\Delta z}{\Delta t}\boldsymbol{R}_S\boldsymbol{C} - \mathbf{1}_n\right]\boldsymbol{V}_1^n - 2\boldsymbol{R}_S\boldsymbol{I}_1^{n+1/2} + \left(\boldsymbol{V}_S^{n+1} + \boldsymbol{V}_S^n\right)\right\} \tag{4.19a}$$

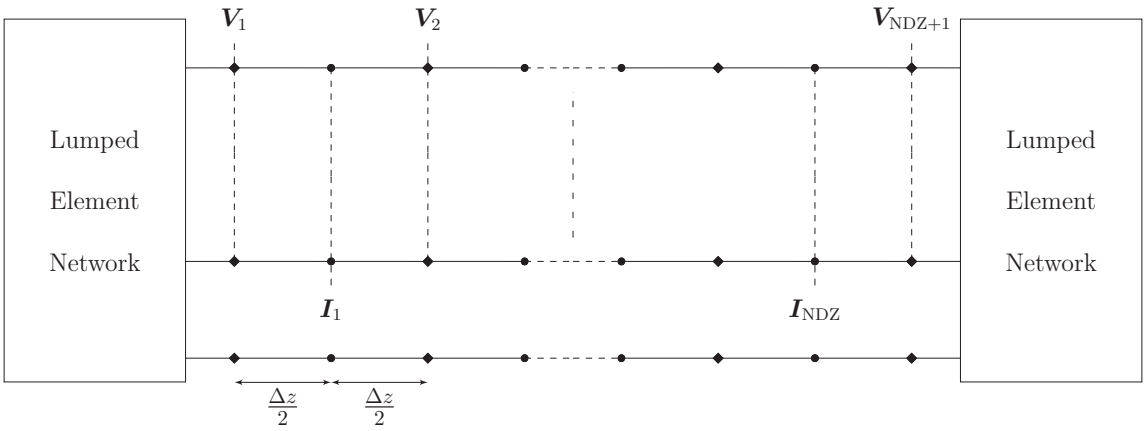

Fig. 4.2: Space desretization of a typical FDTD algorithm for an MTL system.

$$\boldsymbol{V}_{\mathrm{NDZ+1}}^{n+1} = \left[\frac{\Delta z}{\Delta t}\boldsymbol{R}_L\boldsymbol{C} + \mathbf{1}_n\right]^{-1} \left\{\left[\frac{\Delta z}{\Delta t}\boldsymbol{R}_L\boldsymbol{C} - \mathbf{1}_n\right]\boldsymbol{V}_{\mathrm{NDZ+1}}^{n} + 2\boldsymbol{R}_L\boldsymbol{I}_{\mathrm{NDZ}}^{n+1/2} + \left(\boldsymbol{V}_L^{n+1} + \boldsymbol{V}_L^{n}\right)\right\} \tag{4.19b}$$

$$\boldsymbol{V}_k^{n+1} = \boldsymbol{V}_k^{n} - \frac{\Delta t}{\Delta z}\boldsymbol{C}^{-1}\left(\boldsymbol{I}_k^{n+1/2} - \boldsymbol{I}_{k-1}^{n+1/2}\right) \tag{4.19c}$$

$$\boldsymbol{I}_k^{n+3/2} = \boldsymbol{I}_k^{n+1/2} - \frac{\Delta t}{\Delta z}\boldsymbol{L}^{-1}\left(\boldsymbol{V}_{k+1}^{n+1} - \boldsymbol{V}_k^{n+1}\right). \tag{4.19d}$$

$\boldsymbol{V}$ and $\boldsymbol{I}$ are the voltage and current vectors at each space (k) and time (n) descretization. $\boldsymbol{L}$ and $\boldsymbol{C}$ are the PUL inductance and capacitance matrices. $\boldsymbol{R}_s$ and $\boldsymbol{R}_L$ are lumped resistance matrices at the terminals. $\boldsymbol{V}_s$ and $\boldsymbol{V}_L$ are the excitation vectors at each terminal, at each time-step which can be the voltage of series voltage sources or the terminal voltage of a connecting transmission line obtained from a circuit simulator as explained in [46].

Since this technique has originally been developed for parallel multi-conductor transmission lines, it descretizes all conductors in space using a single variable z. However, as (4.19) suggests, for the classical MTL models, the mutual coupling on a segment k is assumed to be caused by the voltages and currents of the responsible conductors, in the same and nearby

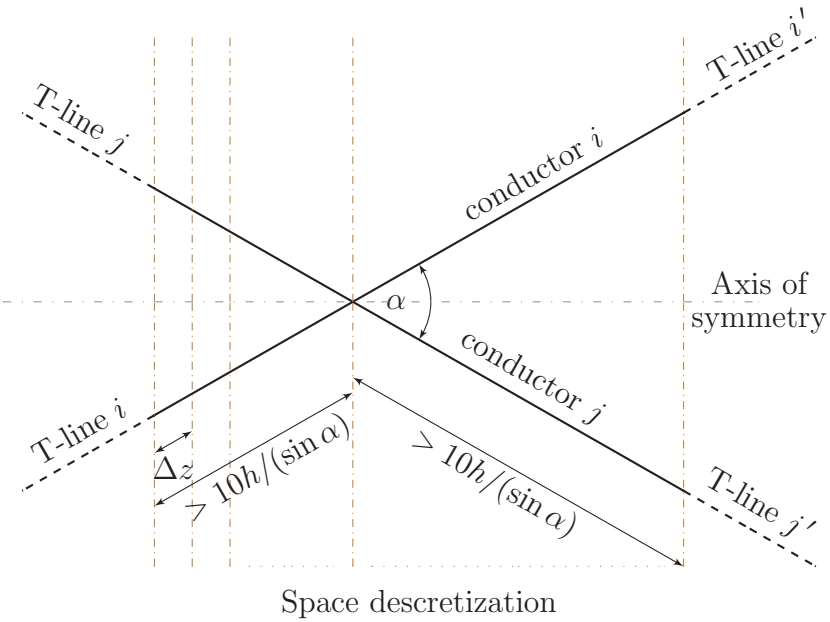

Fig. 4.3: Proposed space desretization of SFTL model for FDTD implementation.

space segments $k-1$, k, and $k+1$. As such, a common variable z is still applicable to the developed SFTL model provided that the modelled structure is symmetrical on the either sides of the crossing, *i.e.* in Fig. 4.1 $c_i = c_j$ and $l_i = l_j$, and the structure is descretized in the format given in Fig. 4.3 in space. This does not affect the end goal of this ongoing research project which is to include SFTL as a circuit component for transmission lines crossings in EMT-type simulators. The region affected by the crossing non-uniformity, which is explained in the next paragraph, would anyway be symmetrical and, the EMT simulators already have the ability to solve non-coupled transmission lines of different lengths (corresponding to T-lines i, i', j, and j' of Fig. 4.3) simultaneously. Equation (4.19) can be used after replacing constant $\boldsymbol{L}$ and $\boldsymbol{C}$ matrices with space-varying $\boldsymbol{L}_k$ and $\boldsymbol{C}_k$.

The effective distance of a current variation on its electromagnetic field is equal to its

wavelength λ [15]. On the other hand, transmission line models are applied for cases where the maximum cross sectional dimension is less than 0.1λ. Therefore, when modelling a long transmission lines with a crossing, the SFTL model should be applied at least for the points that are within a distance of $10h/\sin\alpha$ from the crossing so that all points which are within a distance of $10h$ to each other is modelled using SFTL. This region will be referred to as the critical length herein. The points outside this area can be modelled using classical MTL theory.

4.1.4 Comparison of the Developed Model with a Full-wave Solver

The structure used for the comparison is shown in Fig. 4.4. Conductors were assumed to be cylindrical with a radius of 1 mm. The wire structure was excited with a trapezoidal voltage source (V_s), with a rise and fall time of 0.5 ns as shown in Fig. 4.5. As explained in (4.18), the developed model has space varying PUL parameters due to the non-uniformities along the lines. The whole structure from end to end was modelled using the SFTL (not only the critical region) to include the end effects at the terminals. $L_{11}(z)$ and $C_{11}(z)$ which are analogous to the PUL self inductance and self capacitance of wire 1, and $L_{12}(z)$ and $C_{12}(z)$ which are analogous to PUL mutual inductance and mutual capacitance between two conductors, are shown in Figs. 4.6 and 4.7, respectively. The variation in $L_{11}(z)$ and $C_{11}(z)$ closer to the terminals is due to the change of electric and magnetic fields close to an end of a cylindrical conductor, which is explained in [15]. It is visible how the mutual parameters have an increasing value in areas closer to the crossing. The critical region and magnitude of PUL parameters increases when the crossing angle is decreased, implying a stronger coupling. Figure 4.7 also justifies the choice of $10h/(\sin\alpha)$ as the critical length, which is 0.5 m, 0.29 m and 0.25 m for crossing angles of 30°, 60° and 90° respectively.

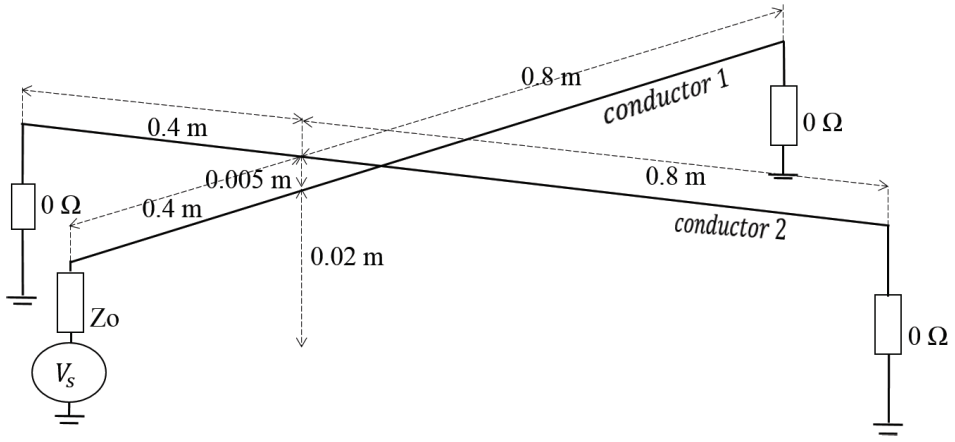

Fig. 4.4: The structure used for the comparison with full-wave theory.

Time-domain results were obtained for crossing angles (α) of 30°, 60° and 90° and compared with those obtained by a full-wave, finite-element (FEM) solver which solves the Maxwell's equations in three-dimensional space. Figures 4.8 to 4.10 show the sending end currents of the excited and victim wires, respectively for different crossing angles.

Both the FEM and SFTL results imply that the crossing causes induced currents on the victim wire as well as reflections on the excited wire. The developed model (SFTL) has been able to capture these interferences occurring on both excited and victim wires, which are not being represented in prevailing power system simulator components. Full-wave results appear to be decaying despite the conductors being lossless and the terminals are short circuited to ground. This is expected to be the radiation loss occurring at the terminals which is not considered in transmission line theory.

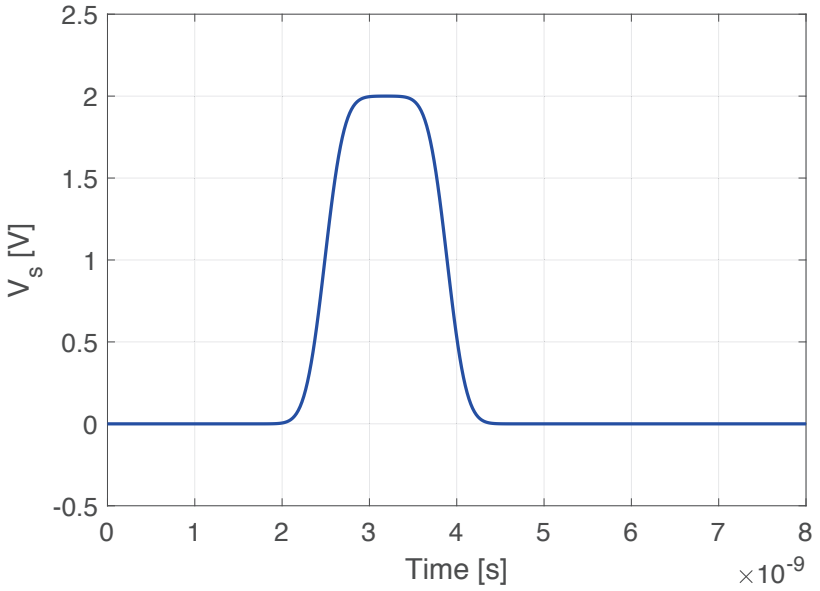

Fig. 4.5: The trapezoidal excitation waveform (V_s) applied on conductor 1.

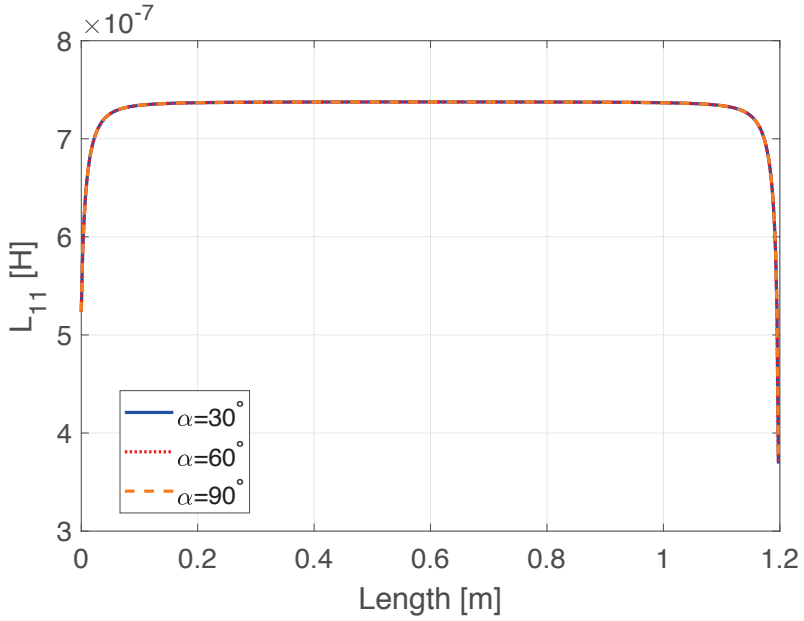

(a)

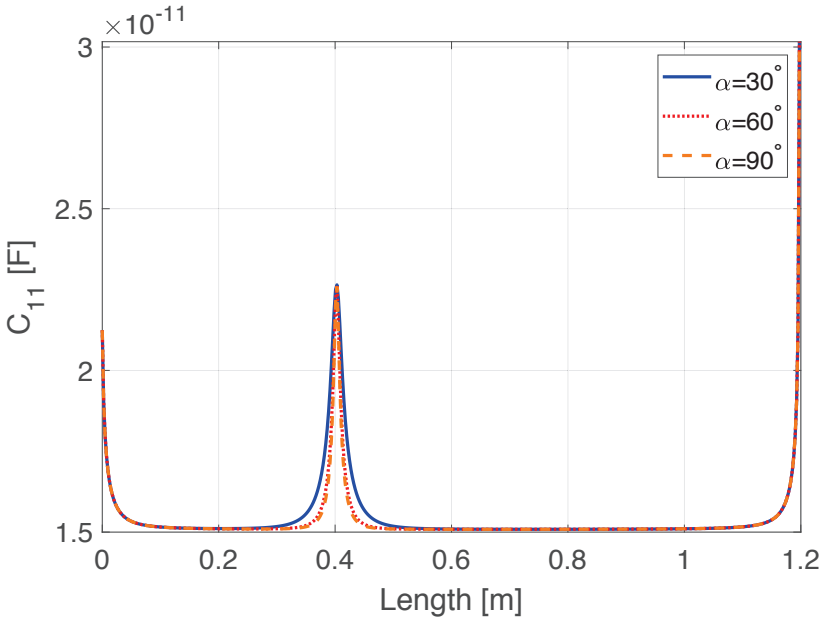

(b)

Fig. 4.6: Self (a) inductance and (b) capacitance of conductor 1 vs z for different crossing angles.

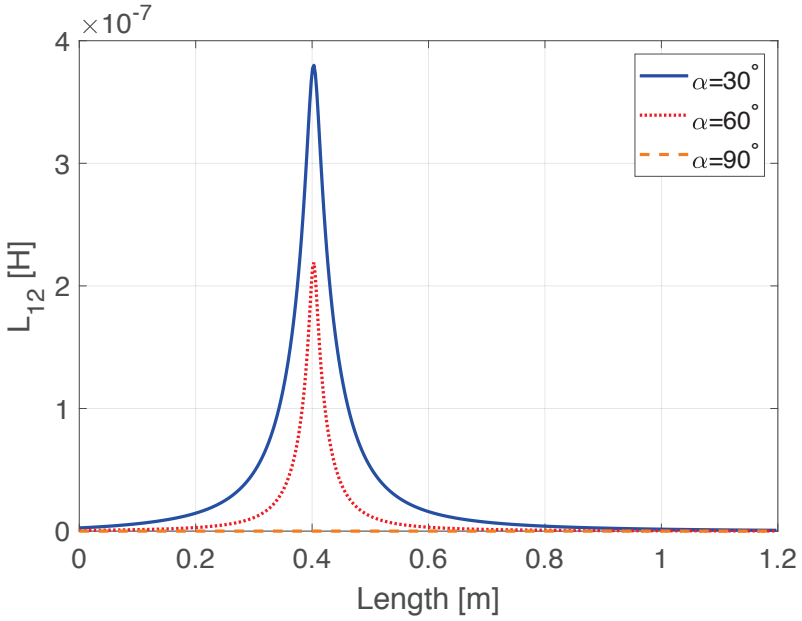

(a)

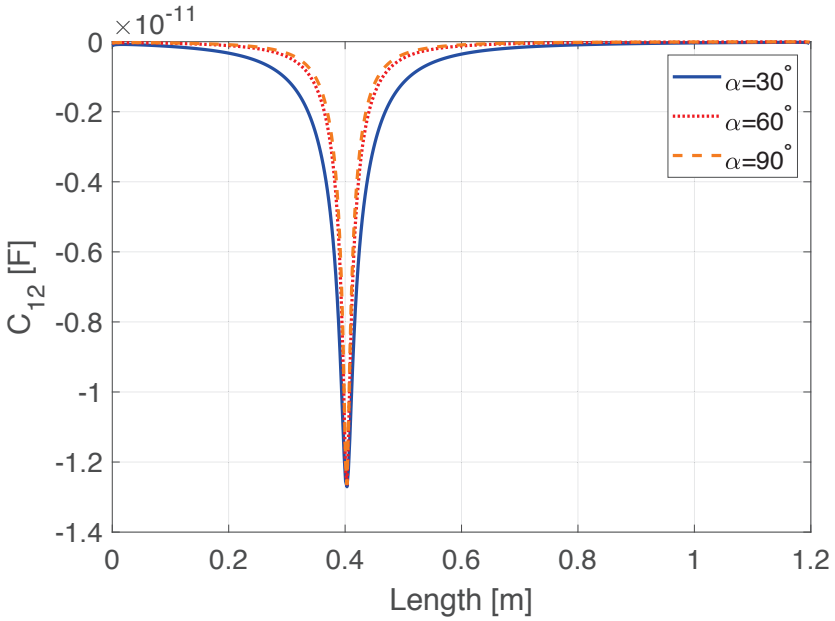

(b)

Fig. 4.7: Mutual (a) inductance and (b) capacitance between conductors vs z for different crossing angles.

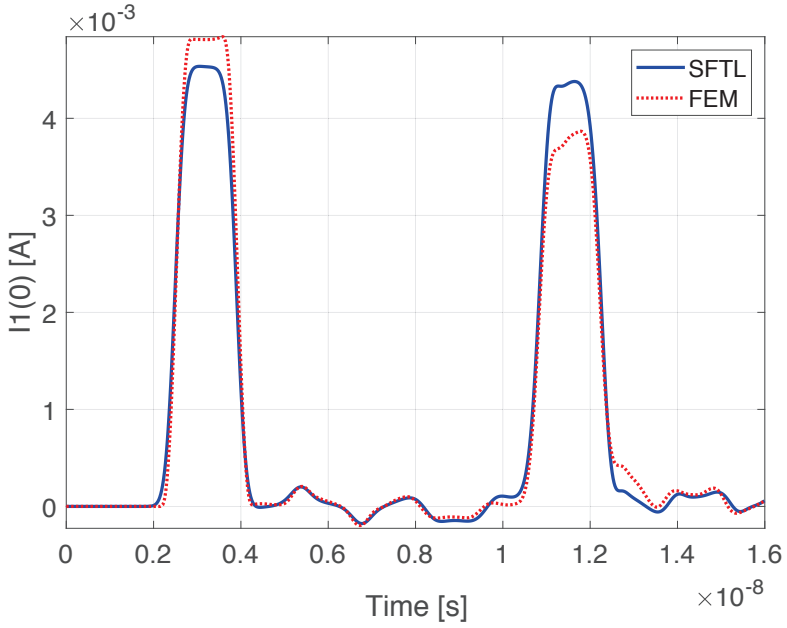

(a)

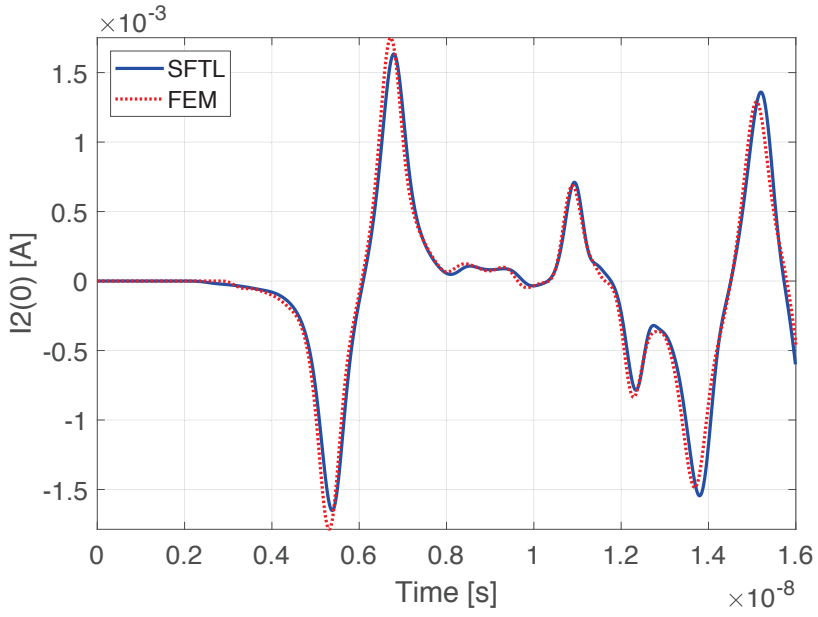

(b)

Fig. 4.8: Sending end currents of (a) excited line and (b) victim line at a crossing angle of $\alpha = 30°$ obtained using the proposed model (SFTL) and full-wave FEM.

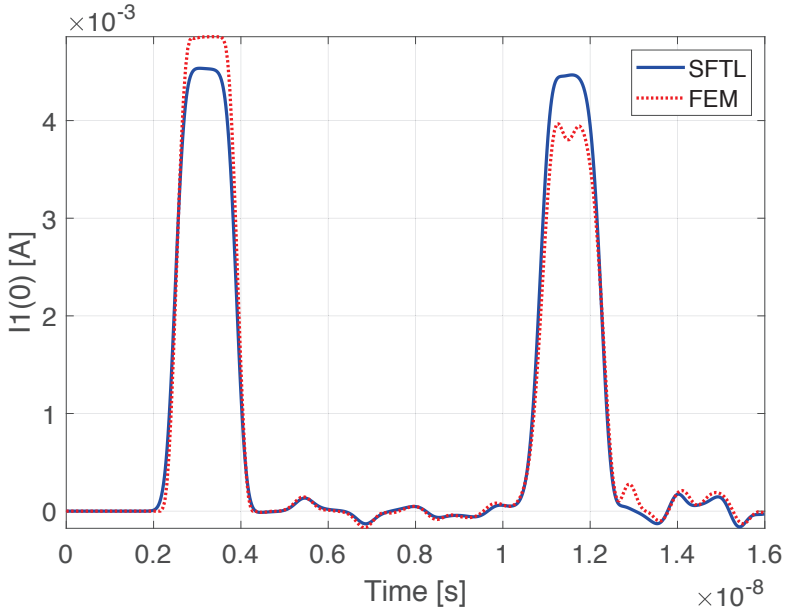

(a)

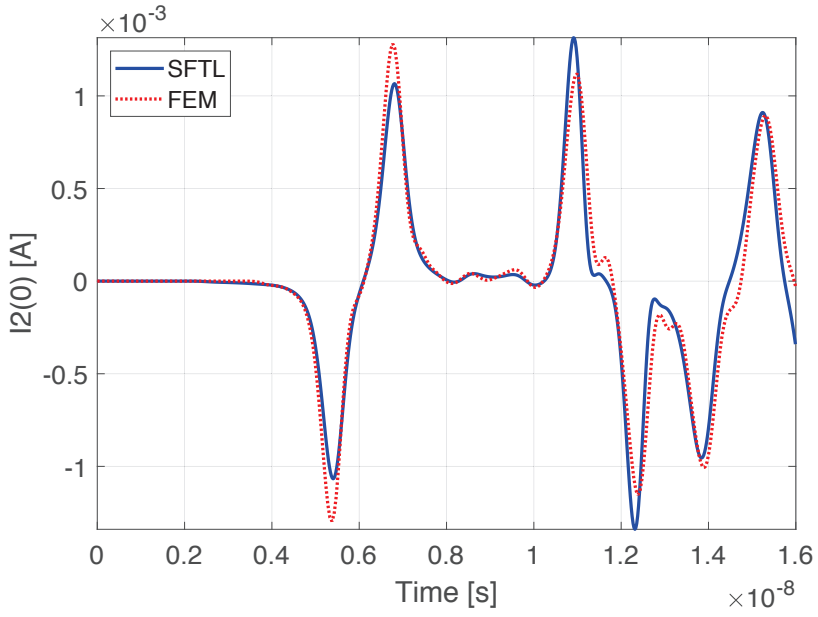

(b)

Fig. 4.9: Sending end currents of (a) excited line and (b) victim line at a crossing angle of $\alpha = 60°$ obtained using the proposed model (SFTL) and full-wave FEM.

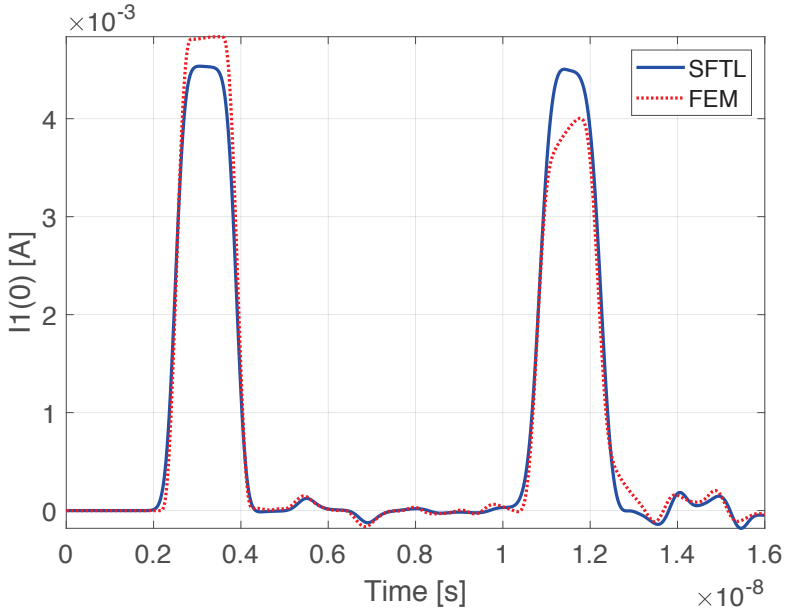

(a)

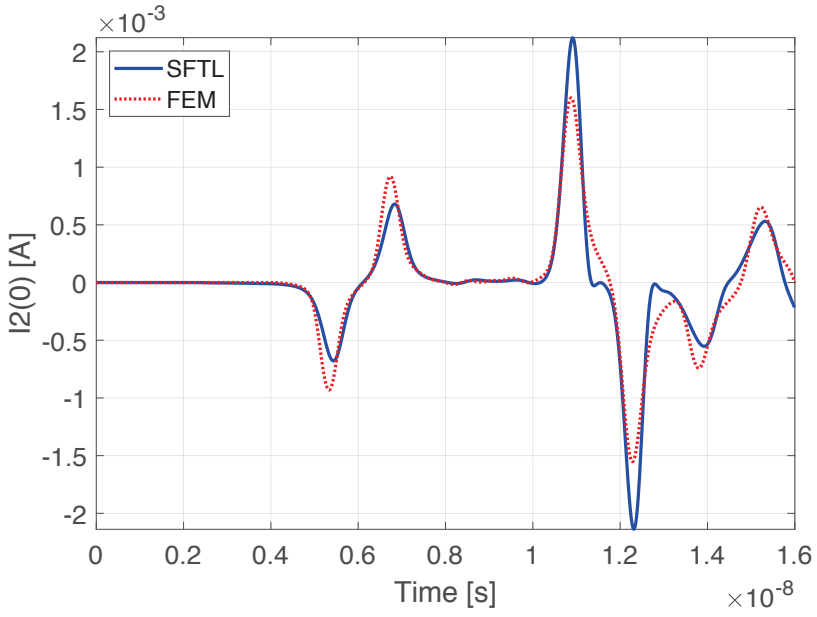

(b)

Fig. 4.10: Sending end currents of (a) excited line and (b) victim line at a crossing angle of $\alpha = 90°$ obtained using the proposed model (SFTL) and full-wave FEM.

4.1.5 Modelling a power line crossing using SFTL

This section demonstrates the changes that should be made to SFTL model if being integrated into an EMT simulator. Dimensions of a typical 500 kV - 230 kV line crossing [53] are used for the structure which was modelled using the SFTL, given in Fig. 4.11. Conductor radii are assumed to be 20 mm. The crossing angle is assumed to be 30°. A trapezoidal pulse with a rise-time of 50 ns [54] and a unit magnitude is set to travel along conductor 1 from A to A'.

Since the SFTL is to be used as a circuit component between crossing transmission lines the end points of the SFTL should not contain the end effect due to a physical transmission line end as in the previous section. Therefore, when calculating $L(z)$ and $C(z)$ in (4.16), instead of integrating from $z = 0$ to $z = \ell$, integral limits were set as, $z = -10\ell$ to 10ℓ. Figures 4.12 and 4.13 show the resulting PUL parameters. It is seen that the effect due to the ends is no longer apparent.

Figure 4.14a shows the trapezoidal pulse travelling along conductor 1, while Fig. 4.14b shows the voltage at point B which occurs due to the induced interference at the crossing. As Fig, 4.14 suggests, a transient of 50 ns rise-time on the 500 kV line can induce an impulse of approximately 8% of the original transient on the victim line at the crossing.

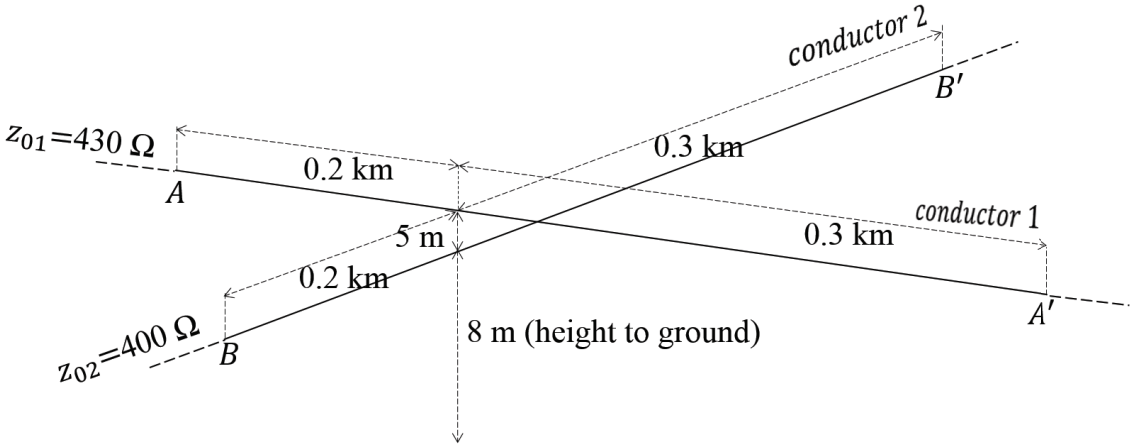

Fig. 4.11: Power line crossing with a crossing angle of 30°.

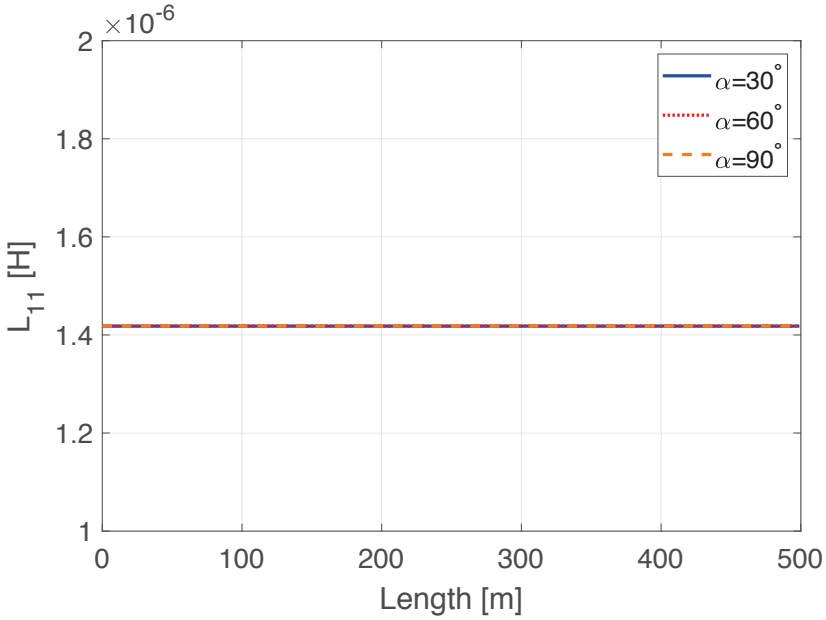

(a)

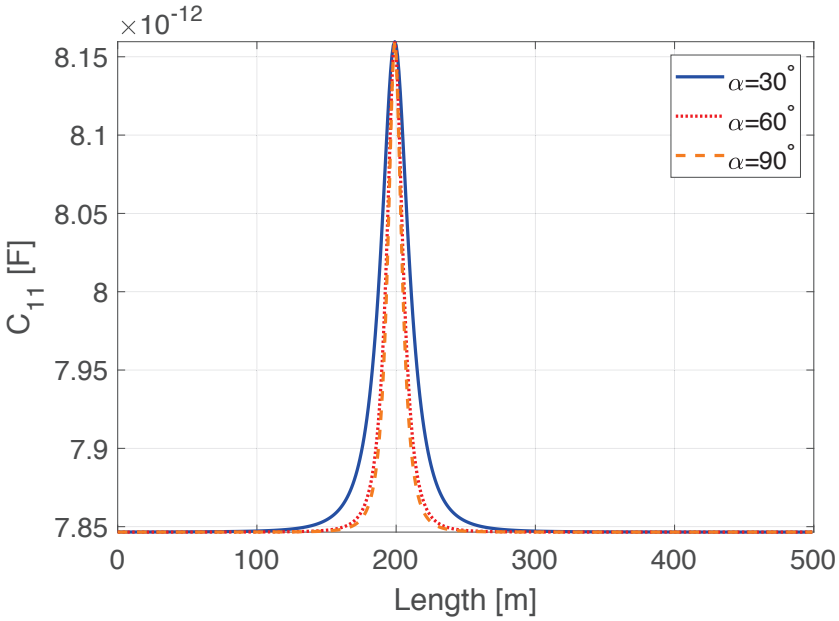

(b)

Fig. 4.12: Self (a) inductance and (b) capacitance of conductor 1 vs z for different crossing angles.

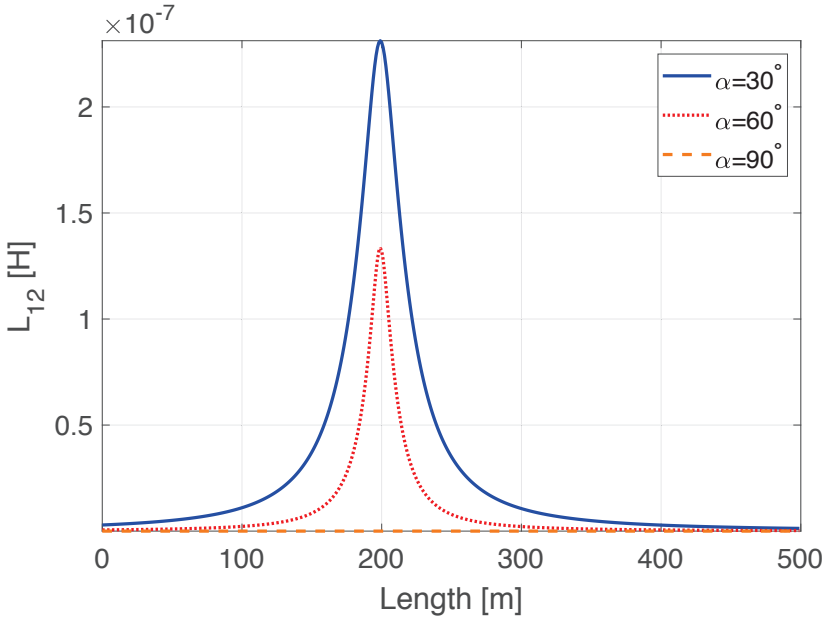

(a)

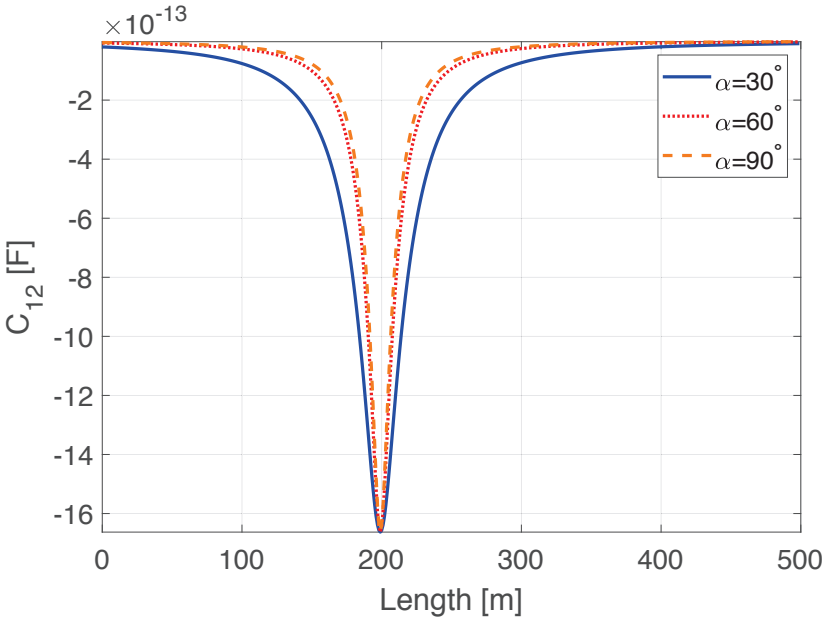

(b)

Fig. 4.13: Mutual (a) inductance and (b) capacitance between conductors vs z for different crossing angles.

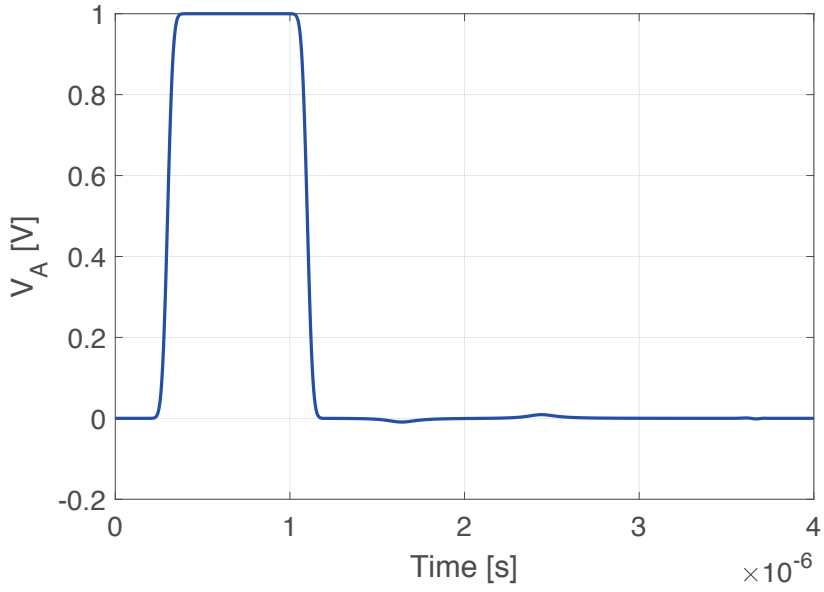

(a)

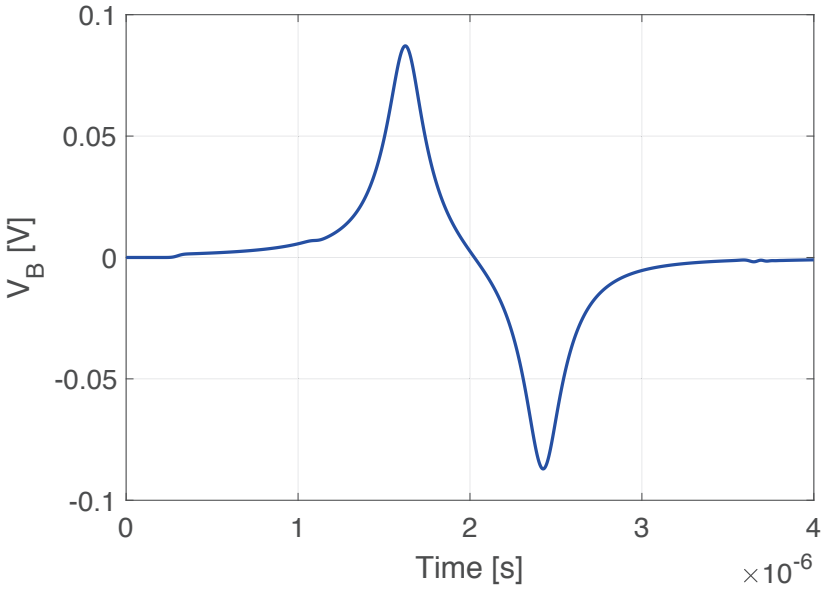

(b)

Fig. 4.14: (a) $V_A(z)$ on the exciter line and (b) $V_B(z)$ on the victim line vs time.

4.2 Scattering Model for a Transmission Line Bend

A model for a single-conductor, lossless, bent transmission line can be formulated using the same approach used for crossings. However in contrast to the crossing, here we assume the coordinate system rotates by an angle equal to the bending angle of the conductor at the location of the bend. Therefore PUL L and C are simplified into different space-dependent functions on the either sides of the bend unlike in the crossing which had a single closed-form function for the entire span of the wire.

4.2.1 Derivation of Scattering Equations for a Bent Wire

For a system as shown in Fig. 4.15, the scattered magnetic vector potential along the axis of the wire and the scalar potential can be expressed as [15]

$$\boldsymbol{A}_z(z) = \begin{cases} \dfrac{\mu}{4\pi}\displaystyle\int_0^b g\left(z,z'\right) I(z')dz' + \cos\alpha\dfrac{\mu}{4\pi}\int_b^\ell g\left(z,z',\alpha\right) I(z')dz' & z \le b \\ \dfrac{\mu}{4\pi}\cos\alpha\displaystyle\int_0^b g\left(z,z',\alpha\right) I(z')dz' + \dfrac{\mu}{4\pi}\int_b^\ell g\left(z,z'\right) I(z')dz' & z > b \end{cases} \tag{4.20a}$$

and,

$$V(z) = \begin{cases} \dfrac{1}{4\pi\varepsilon}\displaystyle\int_0^b g\left(z,z'\right) \rho(z')dz' + \dfrac{1}{4\pi\varepsilon}\int_b^\ell g\left(z,z',\alpha\right) \rho(z')dz' & z \le b \\ \dfrac{1}{4\pi\varepsilon}\displaystyle\int_0^b g\left(z,z',\alpha\right) \rho(z')dz' + \dfrac{1}{4\pi\varepsilon}\int_b^\ell g\left(z,z'\right) \rho(z')dz' & z > b \end{cases} \tag{4.20b}$$

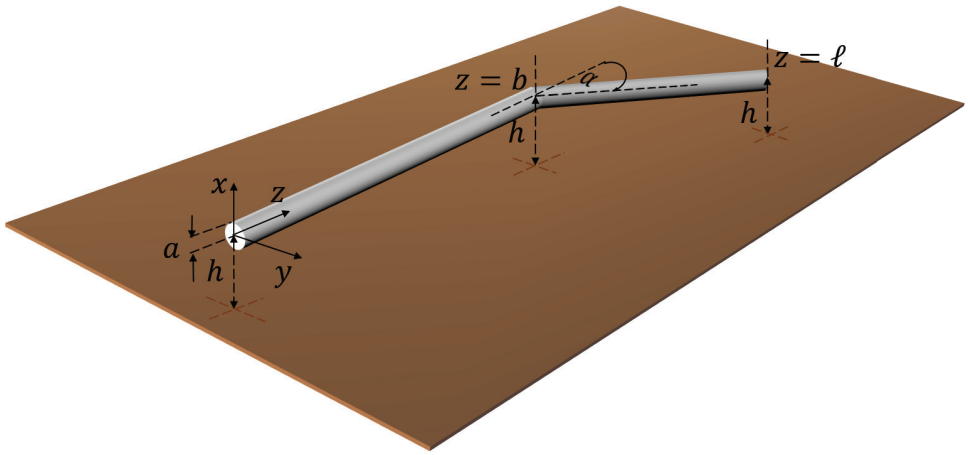

Fig. 4.15: A cylindrical conductor with a bend at $z = b$.

with the variable as defined in Section 4.1.1. Following the same procedure as in Section 4.1, the closed form transmission line like equations can be obtained for a line bend as,

$$\frac{\mathrm{d}V(z)}{\mathrm{d}z} = \begin{cases} -j\omega\dfrac{\mu}{4\pi}\left[\xi_{s,bb}(z) + \cos\alpha\xi_{m,ab}(z)\right] I(z) & z \leq b \\ \\ -j\omega\dfrac{\mu}{4\pi}\left[\cos\alpha\xi_{m,bb}(z) + \xi_{s,ab}(z)\right] I(z) & z > b \end{cases} \tag{4.21a}$$

and,

$$\frac{\mathrm{d}I(z)}{\mathrm{d}z} = \begin{cases} -j\omega\dfrac{4\pi\varepsilon}{\left[\xi_{s,bb}(z) + \xi_{m,ab}(z)\right]} V(z) & z \leq b \\ \\ -j\omega\dfrac{4\pi\varepsilon}{\left[\xi_{m,bb}(z) + \xi_{s,ab}(z)\right]} V(z) & z > b \end{cases} \tag{4.21b}$$

In the ξ terms of (4.21), s or m represents whether coupling is self or mutual, respectively, while bb or ab represents whether the coupling is from the section before or after the bend. The ξ terms, as before, which are the closed-form integrals of the simplified Green's functions,

are given by [52]

$$\begin{aligned}\xi_{s,bb}(z) = &\left[\sinh^{-1}\left(\frac{b-z}{a}\right) - \sinh^{-1}\left(\frac{-z}{a}\right)\right] \\ &- \left[\sinh^{-1}\left(\frac{b-z}{2h}\right) - \sinh^{-1}\left(\frac{-z}{2h}\right)\right]\end{aligned} \tag{4.22a}$$

$$\begin{aligned}\xi_{m,ab}(z) = &\left[\sinh^{-1}\left(\frac{\ell - b + (b-z)\cos(\alpha)}{\sqrt{\left((b-z)\sin(\alpha)\right)^2 + a^2}}\right)\right. \\ &\left. - \sinh^{-1}\left(\frac{(b-z)\cos(\alpha)}{\sqrt{\left((b-z)\sin(\alpha)\right)^2 + a^2}}\right)\right] \\ &- \left[\sinh^{-1}\left(\frac{\ell - b + (b-z)\cos(\alpha)}{\sqrt{\left((b-z)\sin(\alpha)\right)^2 + 4h^2}}\right)\right. \\ &\left. - \sinh^{-1}\left(\frac{(b-z)\cos(\alpha)}{\sqrt{\left((b-z)\sin(\alpha)\right)^2 + 4h^2}}\right)\right]\end{aligned} \tag{4.22b}$$

$$\begin{aligned}\xi_{m,bb}(z) = &\left[\sinh^{-1}\left(\frac{\ell - b + (z-b)\cos(\alpha)}{\sqrt{\left((z-b)\sin(\alpha)\right)^2 + a^2}}\right)\right. \\ &\left. - \sinh^{-1}\left(\frac{(z-b)\cos(\alpha)}{\sqrt{\left((z-b)\sin(\alpha)\right)^2 + a^2}}\right)\right] \\ &- \left[\sinh^{-1}\left(\frac{\ell - b + (z-b)\cos(\alpha)}{\sqrt{\left((z-b)\sin(\alpha)\right)^2 + 4h^2}}\right)\right. \\ &\left. - \sinh^{-1}\left(\frac{(z-b)\cos(\alpha)}{\sqrt{\left((z-b)\sin(\alpha)\right)^2 + 4h^2}}\right)\right]\end{aligned} \tag{4.22c}$$

$$\begin{aligned}\xi_{s,bb}(z) = &\left[\sinh^{-1}\left(\frac{\ell - z}{a}\right) - \sinh^{-1}\left(\frac{b - z}{a}\right)\right] \\ &- \left[\sinh^{-1}\left(\frac{\ell - z}{2h}\right) - \sinh^{-1}\left(\frac{b - z}{2h}\right)\right].\end{aligned} \tag{4.22d}$$

Similar to Section 4.2, the equations for a transmission line bend can be written as

$$\frac{\mathrm{d}V(z, j\omega)}{\mathrm{d}z} = -j\omega L(z) I(z, j\omega) \tag{4.23a}$$

and,

$$\frac{\mathrm{d}I(z, j\omega)}{\mathrm{d}z} = -j\omega C(z) V(z, j\omega) \tag{4.23b}$$

which can be converted into time-domain as,

$$\frac{\mathrm{d}V(z, t)}{\mathrm{d}z} = -L(z)\frac{\mathrm{d}I(z, t)}{\mathrm{d}t} \tag{4.24a}$$

and,

$$\frac{\mathrm{d}I(z, t)}{\mathrm{d}z} = -C(z)\frac{\mathrm{d}V(z, t)}{\mathrm{d}t}. \tag{4.24b}$$

Once $L(z)$ and $C(z)$ are calulated, (4.24) can be easily implemented using a single dimensional FDTD algorithm explained in [4].

4.2.2 Comparison of the developed model with a full-wave solver

The wire structure used for the comparison of results is given in fig. 4.16. The modelled wire is parallel to ground and bent at variable bending angle at a length of 0.3 from the sending end. $L(z)$ and $C(z)$ for different bend angles are given in Fig 4.17. The distortion occurring to the PUL L and C is greater as the bend gets sharper. A Gaussian waveform as shown

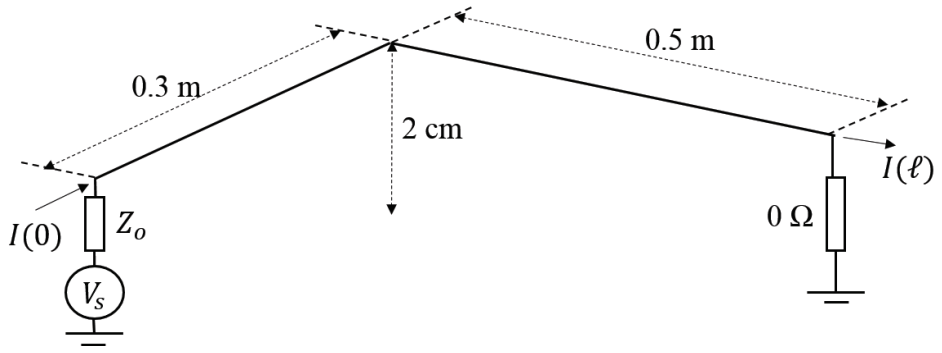

Fig. 4.16: Single-conductor bent transmission line used for the comparison of the SFTL model with a full-wave solver.

in Fig. 4.18 is used as the excitation (V_s). Comparison of the SFTL model for a bend with full-wave results is given in Figs. 4.19 to 4.21. Currents for bend angles of 30°, 60°, and 90° have been presented along with their enlarged first reflection travelling backwards from the bend. As the figures show the SFTL model is well able to produce the reflections occurring due to a transmission line bend which the classical MTL models are incapable of. Similar to the crossing, in the FEM simulation the magnitude of the travelling Gaussian pulse appears to be decaying despite the conductor being lossless and terminated by short-circuiting to ground. This is expected to be due to the radiation occurring at the terminals.

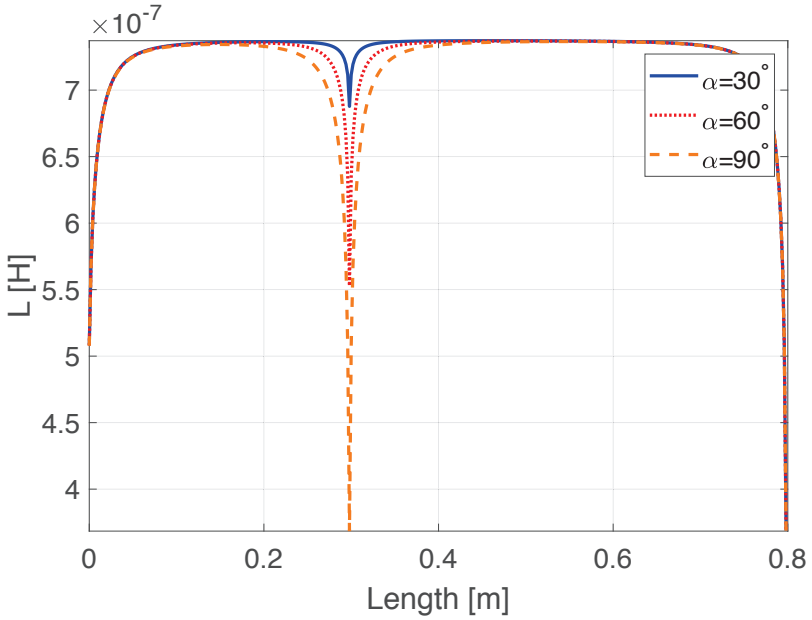

(a)

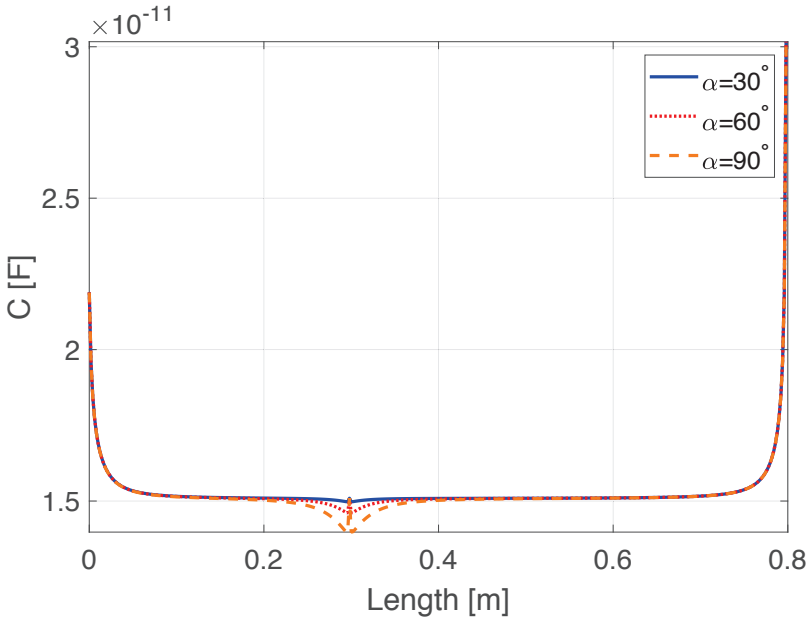

(b)

Fig. 4.17: (a) $L(z)$ and (b) $C(z)$ vs z for different bend angles.

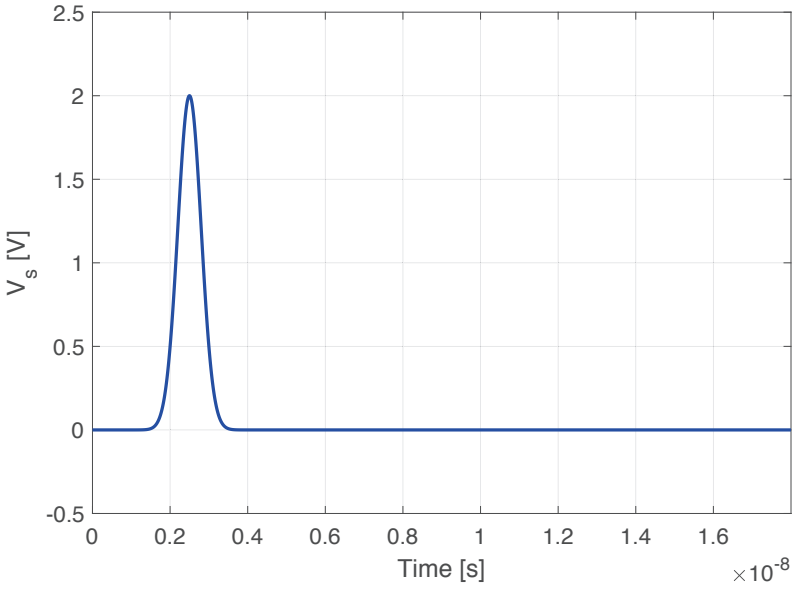

Fig. 4.18: Excitation waveform (V_s).

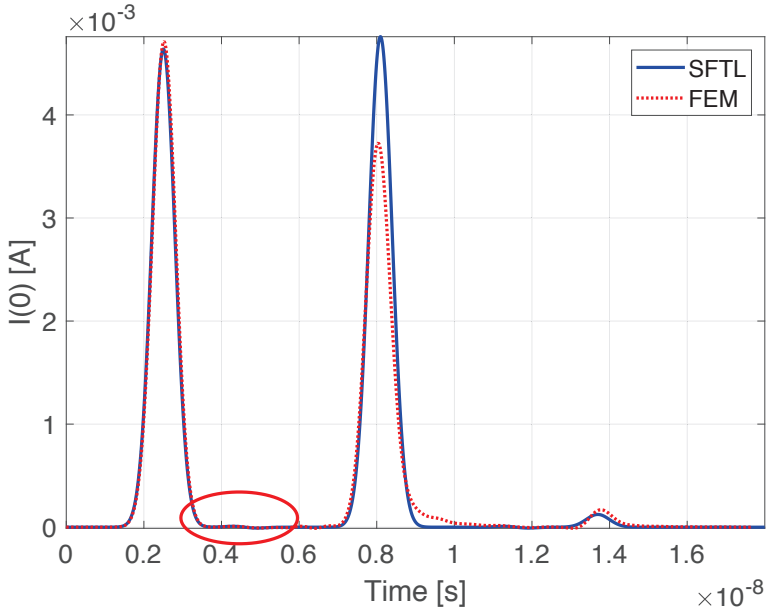

(a)

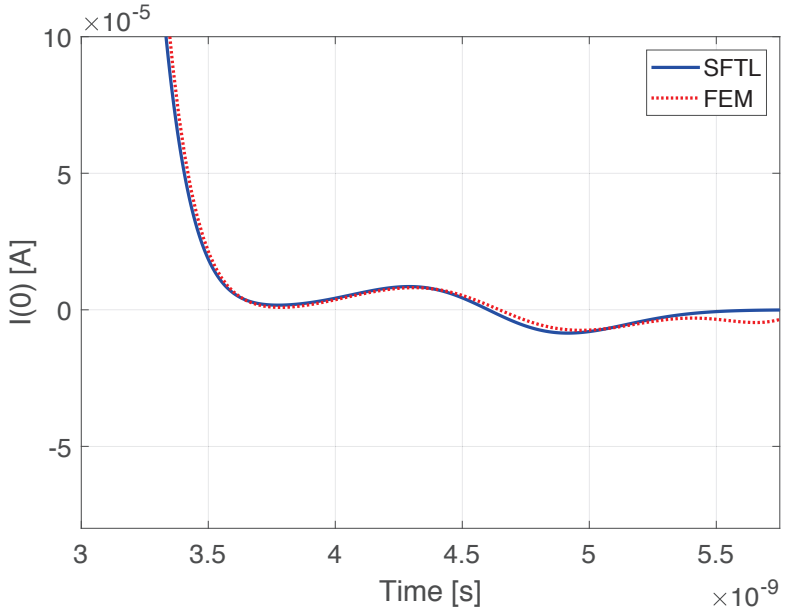

(b)

Fig. 4.19: (a) Sending end current and (b) the enlarged first reflection from the bend for a bending angle of 30° obtained using the proposed model (SFTL) and full-wave FEM.

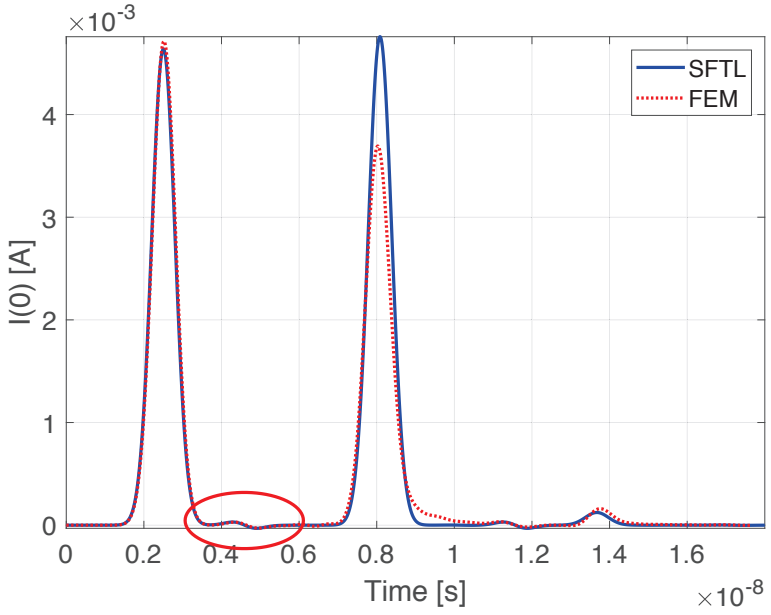

(a)

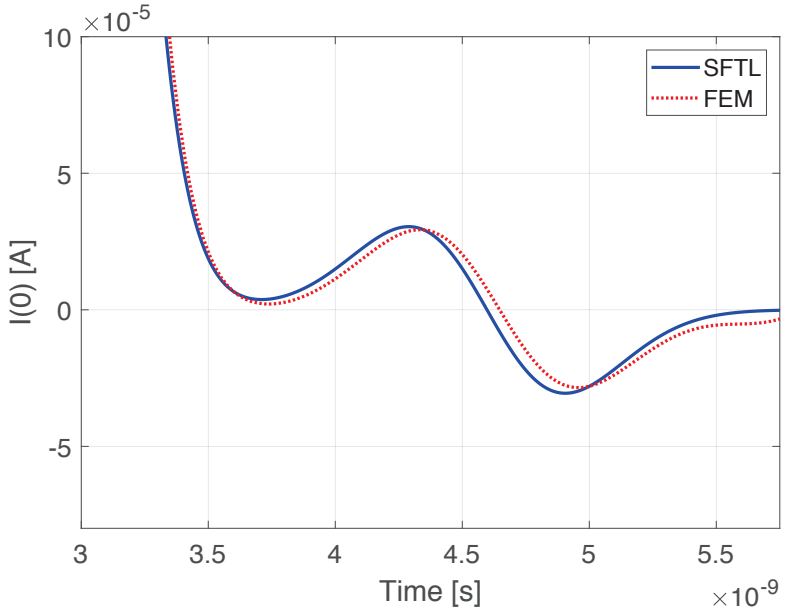

(b)

Fig. 4.20: (a) Sending end current and (b) the enlarged first reflection from the bend for a bending angle of $60°$ obtained using the proposed model (SFTL) and full-wave FEM.

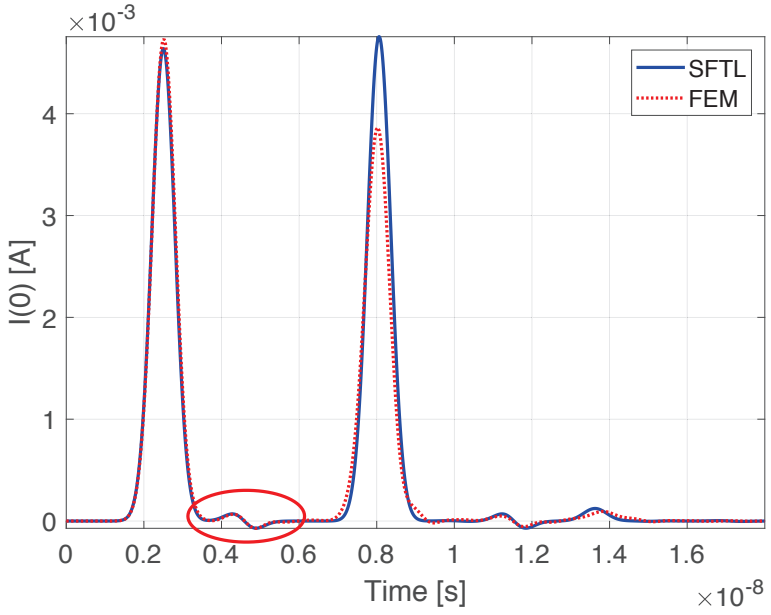

(a)

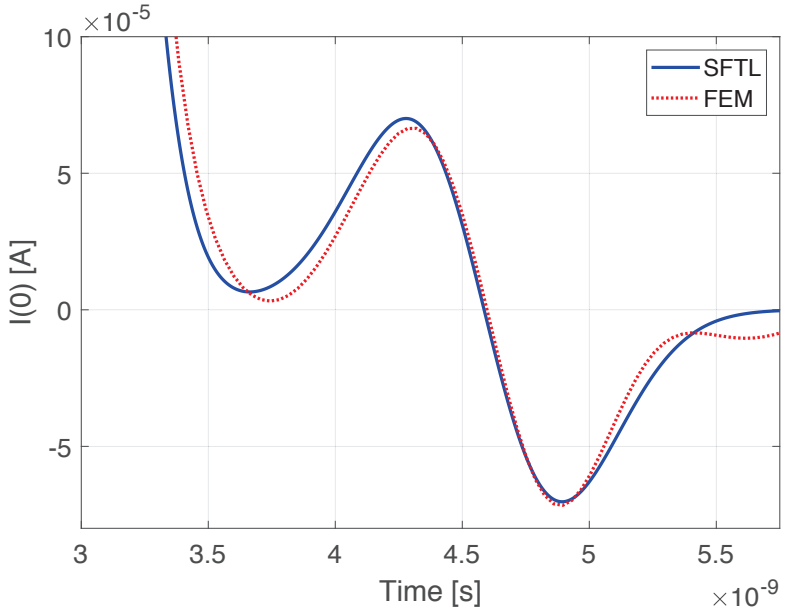

(b)

Fig. 4.21: (a) Sending end current and (b) the enlarged first reflection from the bend for a bending angle of $90°$ obtained using the proposed model (SFTL) and full-wave FEM.

4.3 Summary

In this chapter a closed-form, non-uniform transmission line model was developed which is applicable for the simulation of finite-length lines, transmission line crossings and bends in frequency-independent single-conductor structures. The exciting electric field of non-uniform structures was first formulated using electromagnetic scattering theory and simplified into closed-form equations based on their geometrical and frequency characteristics. The developed model was implemented using a 1D-FDTD algorithm which can be easily integrated into EMT type simulators. Comparison of results obtained from the developed model and a 3D full-wave, finite-element solver, implies that the developed model can simulate the wave distortions occurring due to such non-uniformities. Applicability of the proposed model is currently limited to lossless, thin-wire structures.

Chapter 5
Conclusions

Classical multiconductor transmission line (MTL) theory based on TEM mode of propagation is valid for infinitely-long transmission lines whose cross sectional dimensions are small compared to the minimum wavelength and are uniform along their entire span. Therefore, non-uniformities such as bends, crossings, conductors of different lengths, or electrically distant conductors cannot be represented in classical MTL models. In this research, two enhanced non-uniform transmission line models were developed to model such non-uniformities using the scattering theory.

The proposed scattering-based coupling (SBC) method uses electromagnetic scattering theory to model the mutual coupling between conductors. The SBC model has the ability to model differently-lengthed, electrically-distant, parallel conductors using closed-form equations. The results obtained using the proposed approach for thin-wire, lossless structures have been compared with the Numerical Electromagnetic Code (NEC) which is a full-wave, thin-wire electromagnetic solver. Results have been compared both in the frequency-domain and in the time-domain.

The proposed scattered field transmission line (SFTL) model regards both self and mu-

tual fields as scattered fields and therefore has the ability to represent non-uniformities in single line cases as well. Scattering equations have been simplified into closed-form equations based on geometrical and frequency characteristics used in transmission line theory. The proposed method has been used to model lossless, frequency-independent conductors, that crosses each other at variable crossing angles and for bent conductors at variable bending angles. The SFTL model has been implemented using a finite difference time domain (FDTD) algorithm which is suitable for the integration of the model into EMT simulators as a circuit component. Obtained results have been compared with a 3D-full-wave, finite element solver in time-domain. The proposed model has been able to simulate the reflections and induced currents occurring due to crossings and bends which are not represented in transmission line models currently available in EMT-type simulators.

5.1 Future Work

In this thesis non-uniform transmission line models have been developed and verified for lossless, frequency-independent thin-wire transmission lines. The end goal of this ongoing research project is to develop a circuit component using the SFTL model for EMT type simulators, as the major non-uniformities found in power transmission lines are crossings and bends. In order to be improve the performance of the proposed models the following is suggested.

- Inclusion of losses into SBC and SFTL models as distributed parameters.
- Extension of SBC and SFTL models for frequency-dependent transmission lines. Deriving closed-form formulae for such lines is expected to be a challenging task. Also,

the frequency-domain to time-domain conversion would result in convolution terms which would make the implementation of the model using FDTD much more complex.

- For further verification of the proposed models using experimental results time-domain reflectometry (TDR) tests are suggested.

- As real power lines contain multiple parallel conductors, the current SFTL model needs to be extended for multi-conductor cases before being implemented in an EMT type simulator. Even though, the SFTL model for crossing wires is already for two wires, the p.u.l. parameter calculation will have to be automated for a higher number of wires. In transmission line bends with multiple parallel conductors, the outer conductors being longer than the inner ones is another issue which would have to considered when implementing as a FDTD model.

- Development of a circuit component using the enhanced SFTL model and integration of the circuit model into an EMT-type simulator. Since the SFTL model is currently run on MATLAB, it has to be implemented using a programming language compatible with EMT compilers before being used in an EMT-type simulator.

References

[1] A. J. Martinez-Velasco, *Power system transients : parameter determination.* Boca Raton: CRC Press/Taylor & Francis Group, 2010.

[2] J. Tang, R. Zeng, H. Ma, J. He, J. Zhao, X. Li, and Q. Wang, "Analysis of electromagnetic interference on dc line from parallel ac line in close proximity," *IEEE Transactions on Power Delivery*, vol. 22, no. 4, pp. 2401–2408, Oct 2007.

[3] J. Ma, R. D. Southey, and F. P. Dawalibi, "Measurement and computation of induced noise levels in telephone lines due to harmonics in nearby power lines," in *The 2006 4th Asia-Pacific Conference on Environmental Electromagnetics*, Aug 2006, pp. 577–581.

[4] C. R. Paul, *Analysis of Multiconductor Transmission Lines, 2nd Edition.* Wiley-IEEE Press, 2007.

[5] M. M. Kane and S. V. Kulkarni, "MTL-based analysis to distinguish high-frequency behavior of interleaved windings in power transformers," *IEEE Transactions on Power Delivery*, vol. 28, no. 4, pp. 2291–2299, Oct 2013.

[6] K. Agarwal, D. Sylvester, and D. Blaauw, "Modeling and analysis of crosstalk noise in coupled rlc interconnects," *IEEE Transactions on Computer-Aided Design of Integrated Circuits and Systems*, vol. 25, no. 5, pp. 892–901, May 2006.

[7] R. Achar and M. S. Nakhla, "Simulation of high-speed interconnects," *Proceedings of the IEEE*, vol. 89, no. 5, pp. 693–728, May 2001.

[8] CIGRE, "Brochure 543, guideline for numerical electromagnetic analysis method and its application to surge phenomena, wg c4.501," *CIGRE, June*, 2013.

[9] S. Sakaguchi and M. Oyama, "Application of maxwell solvers to pd propagation. iii. pd propagation in gis," *IEEE Electrical Insulation Magazine*, vol. 19, no. 1, pp. 6–12, Jan 2003.

[10] V. I. Okhmatovski, J. Morsey, and A. C. Cangellaris, "On deembedding of port discontinuities in full-wave cad models of multiport circuits," *IEEE Transactions on Microwave Theory and Techniques*, vol. 51, no. 12, pp. 2355–2365, Dec 2003.

[11] P. Bernardi, R. Cicchetti, and D. S. Moreolo, "A full-wave model for emi prediction in planar microstrip circuits excited in the near-field of a short electric dipole," *IEEE Transactions on Electromagnetic Compatibility*, vol. 37, no. 2, pp. 175–182, May 1995.

[12] T. Uwano, R. Sorrentino, and T. Itoh, "Characterization of strip line crossing by transverse resonance analysis," *IEEE Transactions on Microwave Theory and Techniques*, vol. 35, no. 12, pp. 1369–1376, Dec 1987.

[13] S. Tkatchenko, F. Rachidi, and M. Ianoz, "Electromagnetic field coupling to a line of finite length: Theory and fast iterative solutions in frequency and time domains," *IEEE Transactions on Electromagnetic Compatibility*, vol. 37, no. 4, pp. 509–518, 1995.

[14] S. Tkachenko, F. Rachidi, and J. Nitsch, ""Analytical characterization of a line bend"," *7th International Conference on Computational and Experimental Methods in Eectrical Engineering and Electromagnetics*, vol. 39, no. 1, pp. 599–608, 2004.

[15] F. Rachidi and S. V. Tkachenko, *Electromagnetic field interaction with transmission lines from classical theory to HF radiation effects*. WIT, 2008.

[16] G. Burke, A. Poggio, J. Logan, and J. Rockway, "NEC - numerical electromagnetics code for antennas and scattering," in *1979 Antennas and Propagation Society International Symposium*, vol. 17, June 1979, pp. 147–150.

[17] C. R. Paul, "A brief history of work in transmission lines for emc applications," *IEEE Transactions on Electromagnetic Compatibility*, vol. 49, no. 2, pp. 237–252, May 2007.

[18] C. Taylor, R. Satterwhite, and C. Harrison, "The response of a terminated two-wire transmission line excited by a nonuniform electromagnetic field," *IEEE Transactions on Antennas and Propagation*, vol. 13, no. 6, pp. 987–989, November 1965.

[19] C. R. Paul, "Frequency response of multiconductor transmission lines illuminated by an electromagnetic field," *IEEE Transactions on Electromagnetic Compatibility*, vol. EMC-18, no. 4, pp. 183–190, Nov 1976.

[20] K. S. H. Lee, "Two parallel terminated conductors in external fields," *IEEE Transactions on Electromagnetic Compatibility*, vol. EMC-20, no. 2, pp. 288–296, May 1978.

[21] H. W. Dommel, "Digital computer solution of electromagnetic transients in single-and multiphase networks," *IEEE Transactions on Power Apparatus and Systems*, vol. PAS-88, no. 4, pp. 388–399, April 1969.

[22] *EMTDC Transient Analysis for PSCAD Power System Simulations: User's Guide.* Manitoba HVDC Research Centre, 2005.

[23] H. W. Dommel, *EMTP Theory Book.* Bonneville Power Administration, Protland, OR, 1986.

[24] A. Ametani and M. Aoki, "Line parameters and transients of a non-parallel conductors systems," *IEEE Transactions on Power Delivery*, vol. 4, no. 2, pp. 1117–1126, April 1989.

[25] J. R. Carson, "Wave propagation in overhead wires with ground return," *Bell System Technical Journal*, vol. 5, no. 4, pp. 539–554, 1926.

[26] X. Legrand, A. Xmard, G. Fleury, P. Auriol, and C. A. Nucci, "A quasi-monte carlo integration method applied to the computation of the pollaczek integral," *IEEE Transactions on Power Delivery*, vol. 23, no. 3, pp. 1527–1534, July 2008.

[27] J. Jeong and R. Nevels, "Time-domain analysis of a lossy nonuniform transmission line," *IEEE Transactions on Circuits and Systems II: Express Briefs*, vol. 56, no. 2, pp. 157–161, Feb 2009.

[28] A. Ametani and A. Ishihara, "Investigation of impedance and line parameters of a finite length multiconductor system," *Electrical Engineering in Japan*, vol. 114, no. 4, pp. 83–92, 1993.

[29] A. Ametani and T. Kawamura, "A method of a lightning surge analysis recommended in japan using emtp," *IEEE Transactions on Power Delivery*, vol. 20, no. 2, pp. 867–875, April 2005.

[30] D. K. Cheng, *Field and wave electromagnetics / David K. Cheng.*, ser. Addison-Wesley series in electrical engineering. Reading, Mass.: Addison-Wesley Pub. Co., 1989.

[31] T. Asada, A. Ametani, Y. Baba, and N. Nagaoka, "A study of transient responses on nonuniform conductors by fdtd simulations," *IEEJ Transactions on Electrical and Electronic Engineering*, vol. 11, no. 4, pp. 435–441, 2016.

[32] H. V. Nguyen, H. W. Dommel, and J. R. Marti, "Modelling of single-phase nonuniform transmission lines in electromagnetic transient simulations," *IEEE Transactions on Power Delivery*, vol. 12, no. 2, pp. 916–921, April 1997.

[33] K. Kobayashi, Y. Nemoto, and R. Sato, "Equivalent circuits of binomial form nonuniform coupled transmission lines," *IEEE Transactions on Microwave Theory and Techniques*, vol. 29, no. 8, pp. 817–824, Aug 1981.

[34] A. Cheldavi, "Exact analysis of coupled nonuniform transmission lines with exponential power law characteristic impedance," *IEEE Transactions on Microwave Theory and Techniques*, vol. 49, no. 1, pp. 197–199, Jan 2001.

[35] ——, "Analysis of coupled hermite transmission lines," *IEE Proceedings - Microwaves, Antennas and Propagation*, vol. 150, no. 4, pp. 279–284, Aug 2003.

[36] M. Khalaj-Amirhosseini, "Analysis of coupled nonuniform transmission lines using taylor's series expansion," *IEEE Transactions on Electromagnetic Compatibility*, vol. 48, no. 3, pp. 594–600, Aug 2006.

[37] M. H. Eghlidi, K. Mehrany, and B. Rashidian, "Analytical approach for analysis of nonuniform lossy/lossless transmission lines and tapered microstrips," *IEEE Transactions on Microwave Theory and Techniques*, vol. 54, no. 12, pp. 4122–4129, Dec 2006.

[38] P. Manfredi, D. D. Zutter, and D. V. Ginste, "Analysis of nonuniform transmission lines with an iterative and adaptive perturbation technique," *IEEE Transactions on Electromagnetic Compatibility*, vol. 58, no. 3, pp. 859–867, June 2016.

[39] A. Taflove, S. Hagness, and M. Piket-May, "Computational electromagnetics: The finite-difference time-domain method," in *The Electrical Engineering Handbook*. Elsevier Inc., 2005, pp. 629–670.

[40] A. Tatematsu, "A technique for representing lossy thin wires and coaxial cables for fdtd-based surge simulations," *IEEE Transactions on Electromagnetic Compatibility*, vol. 60, no. 3, pp. 705–715, June 2018.

[41] D. Mardare and J. LoVetri, "The finite-difference time-domain solution of lossy mtl networks with nonlinear junctions," *IEEE Transactions on Electromagnetic Compatibility*, vol. 37, no. 2, pp. 252–259, May 1995.

[42] G. Antonini, A. Orlandi, and C. R. Paul, "An improved method of modeling lossy transmission lines in finite-difference, time-domain analysis," in *1999 IEEE International Symposium on Electromagnetic Compatability. Symposium Record (Cat. No.99CH36261)*, vol. 1, Aug 1999, pp. 435–439 vol.1.

[43] J. Jeong and R. Nevels, "Time-domain analysis of a lossy nonuniform transmission line," *IEEE Transactions on Circuits and Systems II: Express Briefs*, vol. 56, no. 2, pp. 157–161, Feb 2009.

[44] K. Watanabe, T. Sekine, and Y. Takahashi, "A fdtd method for nonuniform transmission line analysis using yee's-lattice and wavelet expansion," in *2009 IEEE MTT-S International Microwave Workshop Series on Signal Integrity and High-Speed Interconnects*, Feb 2009, pp. 83–86.

[45] K. Afrooz and A. Abdipour, "Efficient method for time-domain analysis of lossy nonuniform multiconductor transmission line driven by a modulated signal using fdtd technique," *IEEE Transactions on Electromagnetic Compatibility*, vol. 54, no. 2, pp. 482–494, April 2012.

[46] B. Kordi, J. LoVetri, and G. E. Bridges, "Finite-difference analysis of dispersive transmission lines within a circuit simulator," *IEEE Transactions on Power Delivery*, vol. 21, no. 1, pp. 234–242, Jan 2006.

[47] A. Poggio and E. Miller, "Chapter 4 - integral equation solutions of three-dimensional scattering problems," in *Computer Techniques for Electromagnetics*, 1973, pp. 159–264.

[48] Y. Kami and R. Sato, "Coupling model of crossing transmission lines," *IEEE Transactions on Electromagnetic Compatibility*, vol. 28, no. 4, pp. 204–210, Nov 1986.

[49] S. Park, "Network expression for coupling analysis of arbitrarily directed multiple transmission lines," *Progress In Electromagnetics Research M*, vol. 29, pp. 237–251, 2013.

[50] S. Park, Y. Kami, and Y. Nahm, ""Coupling analysis of complex-layout traces using a circuit-concept approach"," *IEEE Transactions on Electromagnetic Compatibility*, vol. 56, no. 1, pp. 208–220, 2014.

[51] Y. Chunfei, Yim T., Soon, and L. Erping , ""A nonuniform transmission-line approach for modeling bends on transmission lines"," *Microwave and Optical Technology Letters*, vol. 29, no. 1, pp. 71–74, 2001.

[52] S. I. Abramowitz, M., *Handbook of Mathematical Functions with Formulas, Graphs, and Mathematical Tables (Partially Mathcad-enabled).* U.S. Department of Commerce, NIST, 1972.

[53] S. Kalaga and P. Yenumula, *Design of Electrical Transmission Lines : Structures and Foundations.* CRC Press, 2016.

[54] M. Popov, L. van der Sluis, R. P. P. Smeets, and J. L. Roldan, "Analysis of very fast transients in layer-type transformer windings," *IEEE Transactions on Power Delivery*, vol. 22, no. 1, pp. 238–247, Jan 2007.